POLITECNICO DI TORINO

Master of Science program in Physics of Complex Systems

Master's Degree Thesis

Correlation in heart beat time series during exercise

Supervisors
Internal: Prof. Fabrizio Dolcini
External: Prof. Thorsten Emig

Candidate
Giorgio Angelotti
student ID: 248913

Academic year 2018-2019

Summary

Correlations in time series have been widely studied in several fields like biology[9], physiology[10][23], finance[17], signal processing[18], geology[21], astronomy[22], etc. In this internship report we will study the rate variability in heart beat time series recorded during exercise. These time series are generated by physiologic processes that present an intense intrinsic complexity because they are highly non linear and non stationary. We believed that the heart rate variability could be quantified as the behaviour of the fluctuations around a macroscopic trend and with this in mind we will study the time correlations between them. A real time relation between the heart rate variability and the rate could serve to hasten the recovery of patients under rehabilitative treatments and to provide useful information to improve the performances of professional athletes. After a brief introduction, in Chapter 2 I will shed light on the state of the art in the field. For resting time series it has been shown using first fitting an autoregressive process[2][3] and then detrended fluctuation analysis[10][5] that for short time scales the fluctuations are correlated if the time series is recorded from an healthy individual and uncorrelated if they are recorded from a patient who is affected by congenital heart failure. In Chapter 3 I will show why strong trends in RR time series recorded during activity prevent the straightforward application of the previous techniques. I will then interpret anyway the results taking into accounts all the limitations of the used methods[8][11][12][13]. A new analysis approach using the partial autocorrelation function will also be developed in this chapter. An analytical link between all the techniques will be outlined[20], and indeed the results will be consistent between all the methods and will point out that the fluctuations in the studied heart rate regimes are strictly anti-correlated. Anticorrelations are probably born from the coupling of the heart rate with the physiologic vascular regulation and respiration cycles. In the last chapter I will describe a recently invented, data driven algorithm called Empirical Mode Decomposition[26] and its noise-aided versions[27][28] that perform better than Fourier Decomposition on short, non linear and non stationary time series. Its output is consistent with the previously obtained results.

Contents

List of Tables

List of Figures

Above all else, guard your heart,
for everything you do flows from it.

[Book of Proverbs, 4, 23]

Chapter 1

Introduction

1.1 Preamble and motivations

The heart, the most noble of the organs, has been deemed to be, for millennia and in several cultures, the most intimate seat of a person's will, perception and memory.
The word comes from the sanskrit *hṛd*, that is equivalent to the latin *cor, cordis* and to the greek *kardía*. They both share a common indoeuropean root: *skar, skard* that means *to vibrate, to bounce, to jump*.
The whole history of mankind comes as the offspring of this small little engine, whose relentless movement serves as a perfect allegory of life itself. Indeed, never ceasing to pulsate, by its alternating vibrations, thoughts were born, passions bloomed and decisions made.
It's only in the eighteenth century, when a rigorous scientific method was applied to physiology, that the heart lost his primate as the center of thoughts in favour of the brain. Nevertheless, in our cultural heritage and language, it has never lost his former role and will never be a mere pump for blood. When we feel sad after breaking up with a partner, we still say that *he/she broke our heart*; when we memorize an expression we still do it *by heart* and when we are striving for excitement, we are looking for something that makes our *hearts beat faster*.
In the light of the previous statements, the purpose of this thesis is to study both *quantitavely* and *qualitatively* correlations and fluctuations in the heartbeat time series, not only driven by scientific motivations, but also guided by the same zeal that made young men love and poets dream.

1.2 Heart Rate Variability

The object of this work will be a quantity called *Heart Rate Variability* or *HRV* that characterizes the state of the variations in a heartbeat time series and that also describes the propensity of the heart to adapt both to external and internal stimuli. Previous studies

showed that changes in HRV affects the health status and, solely by determining the HRV, one can classify healthy individuals and patients that suffered from a heart failure[5][10]. All of this suggests that the classical concept of homeostasis should be redefined: homeostasis is not meant to allow the body to keep a fixed state, but grants it to adapt to changes without failing[5]. Unfortunately, at the current day, HRV does not have an unequivocal definition, but many quantities have been candidated to fill this position: the ARV (Auto Regressive Variability) that points how well an autoregressive model fits the time series[2][3] and the Hurst exponent H describing the rate of decay of the autocorrelation function along a time series at long timescales[7]. Focusing on details, for time series we will consider the ones made of RR intervals, namely the periods of the time interval that spans two adjacent R peaks in an electrocardiogram measurement (Figure 1.1).
With this in mind, in the next pages I will outline the first attempts of estimating the HRV

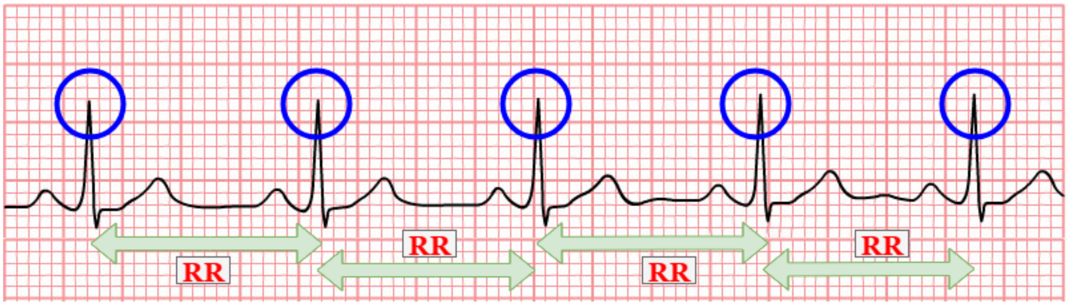

Figure 1.1: How the RR time series is constructed starting from an ECG recording. First the R peaks (circled in blue) are individuated, then their distance (the length of the green segments) is computed. Each entry of the RR time series is the distance between two adjacent R peaks.

from the time series of resting subjects. Specifically, I will illustrate the pros and contra of fitting an autoregressive (AR) model to the RR time series and afterwards I will also shed light on the method called *Detrended Fluctuations Analysis* or *DFA* which estimates the Hurst exponent exploiting a remarkably, approximately, present scale invariance property of the data. With our hearts strengthened by the appealing beauty of the results obtained by DFA on resting individuals, we will then apply the same method to RR time series of running athletes during exercise. As we will see, in this case more hindrances will arise, the greatest of them all being the not-anymore negligible or easily treatable trends.
Let us begin!

Chapter 2

Heart Rate Variability at rest

This chapter is about the current state of the art in the field. For more details about the recording devices and samples see the related references.

2.1 Resting time series

The ECG of several volunteers at rest was recorded during a whole day. By at rest we mean that during the day the patients just experienced a sedentary life with little physical activity, like slowly walking for little distances. According to the AHA[4], a resting heart rate is comprised between approximately 60 and 100 bpm (beats per minute). Since usually the measurement devices record the RR time series with a sensibility of 1 *ms*, the latter can be converted to the time series of instantaneous Heart Rate (HR) with the proper expression:

$$\mathrm{HR}(i) = \frac{6 \times 10^4}{\mathrm{RR}(i)} \frac{\mathrm{bpm}}{\mathrm{ms}}$$

where i is the element (beat) number along the time series.
If the subject is not involved in any intense physical activities its heart rate will vary slowly within the given range. A 24h record will generate a time series of $\approx 9 \times 10^3$ entries. (Figure 2.1)

2.2 Why Fourier decomposition is not enough

The vademecum of the good time series analyst prescribes to perform a Fourier decomposition with the aim of investigating which ones are the main frequencies that characterize the spectrum of the data. From that one could extrapolate one relation linking the frequencies, the shape of the spectral density function or the autocorrelation function to the HRV.

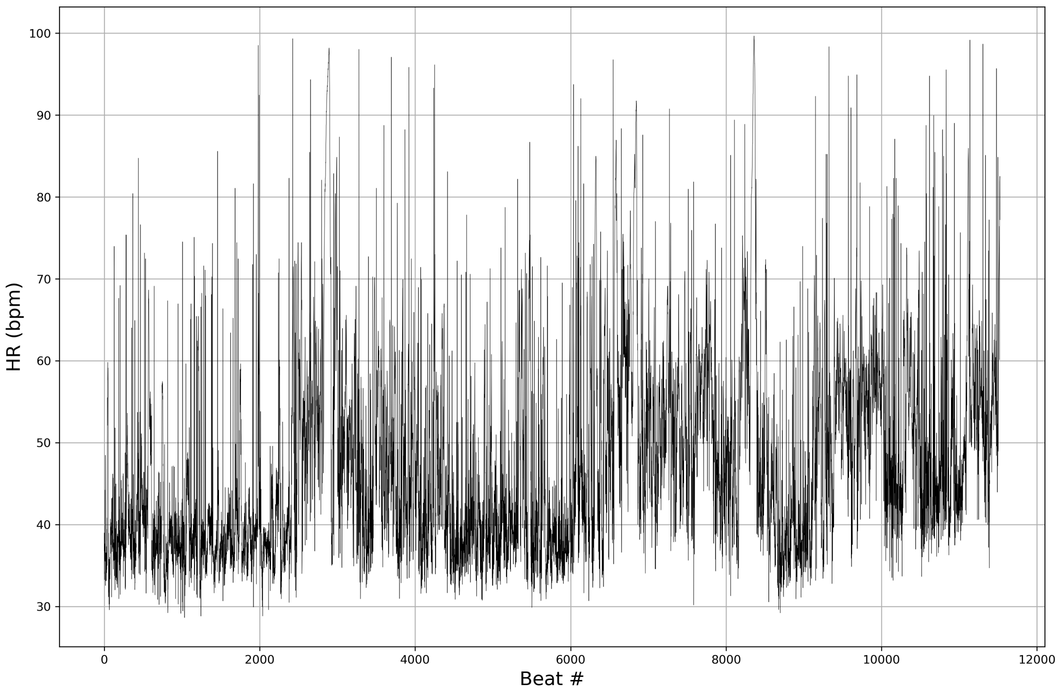

Figure 2.1: HR time series of a patient at rest during 3h.

Fourier Spectral Analysis, in order to give consistent results, requires the data set to have two important properties:

1. The system generating the data must be linear
2. The time series must be strictly periodic or stationary

Indeed, for a *stationary* signal, the Wiener–Khinchin theorem is valid[1] and the following relation for the autocorrelation function $R(\tau)$ holds:

$$R(\tau) = \mathbf{E}\left[\mathrm{RR}(i)\mathrm{RR}(i-\tau)\right] = \int_{-\infty}^{\infty} S(f)e^{i(2\pi f)\tau}df \tag{2.1}$$

where $R(\tau)$ is the autocorrelation function and $S(f)$ is the Power Spectral Density function.
We notice that $S(f)$ is related both to the Fourier transform of $R(\tau)$, both to the squared modulus of the Fourier Transform of RR.
Therefore, in order to study the rate of decay of R, one could:

1. Compute directly the expected value in (2.1)
2. Analyze the behaviour of $S(f)$ obtained by Fourier transforming RR

Remark 1 *It is known from physiology that the heart rate is coupled with many regulatory systems that act at different frequencies, often varying with time. It is believed the existence of a coupling with the respiratory cycle and of some mechanisms that adjust the heart rate according to the intensity of the physical activity, to the variations in the blood pressure and body internal temperature. One could try to model the heart rate as a system of coupled stochastic differential equations where also the strength of the couplings itself varies with time. It goes without saying that the* complex system *is way too hard to model and analyze. Therefore it works better to consider the heart as a* black box *and try to extract useful quantities directly from the recorded time series ignoring the physiologic rhythms. Nevertheless, when we draw our conclusion, we must not forget that the presence of these regulatory oscillating feedback loops will be reflected in some peaks in the power spectral density function (and hence in some periodicity in the autocorrelation function) and therefore they could affect our estimate of the decay rate of the correlations along the time series.*

Unfortunately, our time series are *non-stationary*. Strictly speaking, the cumulants related to the probability distribution from which the series entries are extracted could change with time. Or, using a better definition, the process is not time translation invariant.
More specifically we can say that a time series X is stationary if the following relations hold:

$$\mathbf{E}\left[\left|X(i)^2\right|\right] < \infty \tag{2.2}$$

$$\mathbf{E}\left[X(i)\right] = m \tag{2.3}$$

$$C\left(X(i), X(j)\right) = C\left(X(i+\tau), X(j+\tau)\right) = C(i-j) \qquad \forall i, j \tag{2.4}$$

Non-stationarity is evident because there are trends in the data.
We define as a trend the whole set of variations in the time dynamics that do not depend of the inner regulatory systems, but are a direct consequence of a decision made by the person or caused by external factors e.g. starting accelerating or walking causes a saturating exponential increase in the heart rate [15].
Additionally, we can't state that the process generating the signal is linear, and just to worsen the scenario the finite number of points available in a time series creates artifacts in the Fourier spectrum. Also other problems can arise: in fact the Fourier transform employs *globally* uniform harmonic components. If the signal is non-stationary and/or non-linear, and therefore only *locally* defined, the Fourier decomposition might need additional harmonics to describe it, and hence the energy of a non-stationary local signal will be spread unto a much wider range of frequencies that, in principle, are not physically excited in the data, only to ensure the mathematical rigor of the deconstruction. Even so, Fourier spectral analysis is still used to study non-stationary and non-linear time series due to lack of alternatives. Nevertheless, one should take all these aspects into account in order to adopt this tool.

Remark 2 *In order to obtain an estimate of the rate of decay of the correlations it's mandatory at least to* detrend *the time series in the sense of transforming the data set in one with identical fluctuations around a zero or constant instantaneous mean value.*

Since the form of the trend is unknown it's up to the analyst to decide what really is a trend and what are the fluctuations, hoping that the choice will lead to consistent results. Techniques as DFA include an intrinsic detrending scheme by fitting a polynomial [9]. In the final chapter another detrending procedure based on an algorithm called Empirical Mode Decomposition and the subsequent Hilbert-Huang spectral analysis will also be explored [26].
Keeping in mind the limitations of Fourier Spectral Analysis we will procede adumbrating two different approaches that have been used to study correlations in RR resting time series: fitting an AR model and DFA.

2.3 AR model fitting

In the '80s a Japanese research team proposed an innovative technique to detrend and study the heart rate variability[2][3].
Firstly, they define a sliding window of width N to be moved along the data with a step of size n. Secondly, they fit the autoregressive model of order p^* where both p^* and the coefficients of the model are chosen with the goal of minimizing the AIC (Akaike Information Criterion). Let's remember that an autoregressive process X of order p is defined in the following way[18]:

$$X(i) = \sum_{j=1}^{p} a_j X(i-j) + \xi_i \tag{2.5}$$

where the a_j coefficients show the intensity of the lagged effect on the value of the series at time i enforced by the values assumed by the series at times $i - j$. ξ_j is a Gaussian random variable of zero mean and variance one.
Let then RR^* be the average time series given by the optimal AR fit (in the sense of minimizing AIC) of RR, we can define a residual time series Z as:

$$Z(i) = \mathrm{RR}(i) - \mathrm{RR}^*(i) \tag{2.6}$$

A quantity called Auto Regressive Variability for the AR model of order p, ARV(p), is straightforwardly defined as:

$$\mathrm{ARV}(p) = \frac{\mathrm{Var}\,[Z]}{\mathrm{Var}\,[\mathrm{RR}]} \tag{2.7}$$

Since, by construction, Z is the residual series obtained by subtracting the fit from the RR time series, equation 2.7 establish a sort of normalized fit error that can assume values between 0 (if the fit is perfect) and 1 (in case the fit is useless).
Moreover, if the a_j are such that the roots of $\Phi(z) = 1 - \sum_{j=1}^{p} a_j z^j$ reside out of the unit circle in the complex plane, then the AR process will be linear and stationary in a

wide-sense[18].
The fitting procedure is hence a way to project a process that is non-linear and non-stationary into one that can be examined with the Fourier spectral analysis. Of course, while doing so, we might be losing many important details.

Remark 3 *Interpreting the results, in [2][3] it is claimed that high ARV corresponds to high heart rate variability. However, a great fitting error indicates that the deterministic behavior exerted by an AR process is too simple to describe a more complex inner dynamics. We must acknowledge hence that identifying ARV as a marker of the HRV is most probably an oversimplified interpretation.*

Although the results of [2][3] may become questionable for high ARV, the evolution of the Fourier-PSD of the sliding window along RR* is still interesting to look at because now we can supplement it with a parameter that tells us how reliable the interpretation is. Choosing the more comfortable units of beats instead of seconds for the time, $S_{\mathrm{RR}^*(i),N}(f)$ clearly shows peaks around $f = 0.50$ beats^{-1}, 0.25 beats^{-1}, 0.10 beats^{-1} and 0.05 beats^{-1} that should be respectively related to the physiologic feedback loops of sinus arrhythmia, respiration, regulation of blood pressure and temperature which is concerned with the vascular motion (Figure 2.2) The peaks evolve with time in a non-trivial way. Their average frequency shifts and both their amplitude and spread can increase or decrease. An interesting result is that for patients at rest the spectrum contain most of its power in a low frequency band ($f < 0.1$ beats^{-1}), while in patients that suffer of cardiac diseases such as atrial septal defects and arrhythmias like atrial fibrillation and ventricular premature beats have large amount of power at high frequency band.
The AR fitting approach has been applied also to RR time series of running athletes during exercise. An AR process that simulates frequency excitations related only to the respiration peak was first extracted from the original fit. Subsequently it was shown how the ARV(p) of this constructed respiration-related time series increases with a boost in the heart rate. In running time series most of the power was contained in a frequency band around 0.5 beats^{-1}.
The author's conclusion is then that the HRV increases with the intensity of the exercise, while, as we have seen, a more plausible statement would have been that in this regime the AR model cannot well describe the process.
Fitting and then drawing the conclusion from the fit is a very contrived method that can be both computationally expensive, both can lead to unphysical results since the analyzed time series will be different from the starting one. The detrending perpetuated while doing so neither is well under control: we know that some details are lost but not exactly which ones and in what extent.

2.4 Self-similarity and DFA

The urge for a less invasive detrending was henceforth greatly felt by the scientific community. Surprisingly, Goldberger, Stanley et al.[10][5], discovered that the trajectory that

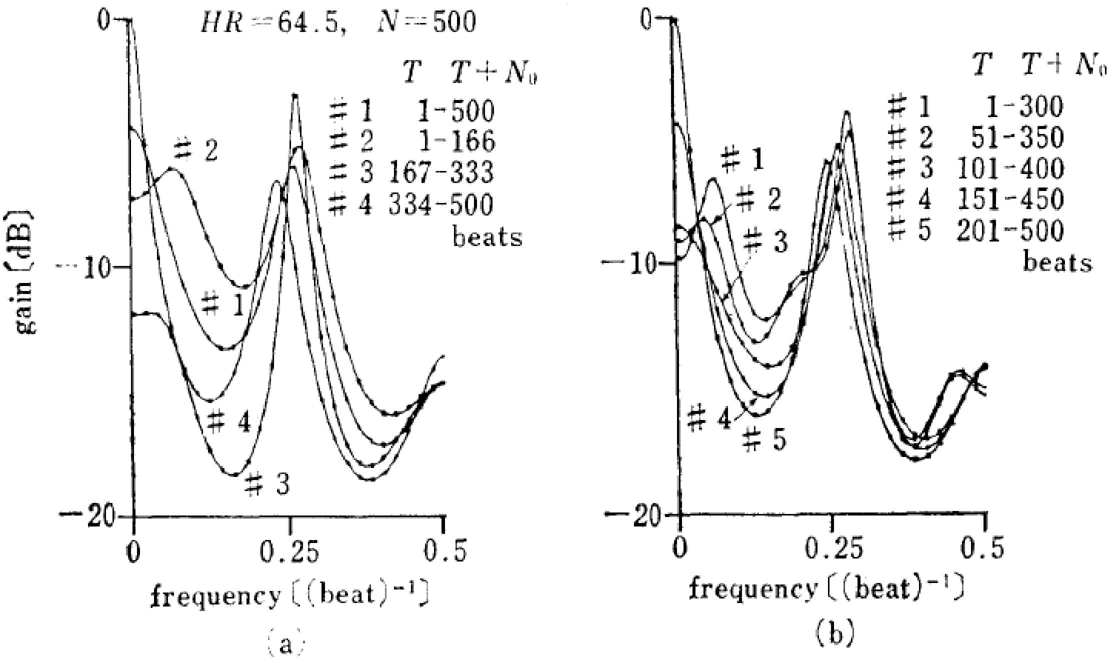

Figure 2.2: Fourier Spectrum along a resting time series of a young girl with average HR=64.5 bpm. On the vertical axis is reported, in decibels, the log ratio between the power contained in the signal at a specific frequency and the maximum energy related to any frequency and any sub-time series. The Power Spectral Analysis is computed in sub time series along the original one going from beat index T to beat index $T + N_0$. Taken from [2].

one can build up from the RR time series approximately benefits from *self-similarity*, a particular property that arises when the underlying process is scale-invariant, even though only in a statistical way. The immediate general idea was then to exploit this feature to infer some relations about the nature of the fluctuations in the data. In order to clarify how the method works it might be useful then to remember the key concepts of self-similarity, scale invariance and how they affect the correlation function.

2.5 Self-similarity

An object is said to be self-similar if upon both a multiplication by a specific coefficient and a scaling transformation of the coordinate system its structure is preserved exactly or approximately[6].
Quantitatively, let $f : \mathbb{R} \to \mathbb{R}$ be a function describing some physical property of an object, then f is said to be self-invariant if the structure is exactly preserved:

$$f(\lambda x) = \lambda^{\Delta} f(x)$$

Fractals are a perfect archetype of self-similarity.
In nature an infinite rescaling towards both smaller and smaller or larger and larger scales is impossible due to the trivial limits given by discretization in the first case and finite size in the other.
Therefore we will say that there exist fractals only in a statistical sense. Up to a given rescaling threshold some functions describing the properties of a fractal will not represent identical patterns, but only statistical similar ones. The exponent Δ is called the *fractal dimension* of the object and it can be different from the intuitive definition of dimensionality. According to the Hausdorff definition Δ is a statistical property that defines how much the fractal fills the space where it is embedded.
Δ is not exclusively a constant and can depend on the scale λ. In this case we can say that the object is not a simple fractal, but a multifractal. Usually in physics scales are fundamental: what happens at a macroscopic scale is different from what is happening at Planck length scale. Anyway scale-invariance and self-similarity are common characteristics in statistical physics when the models, in their range of validity, are describing systems that exhibit a critical behaviour.
At the critical point of some control parameter usually phase transitions happen and *correlations* in the system become infinite at any distance. Nearby the critical point the correlation function decays as a power-law, the only kind of function that suffice the requirements dictated by scale-invariance. Therefore, within the range of validity of the statistical model that describes it, a system at one of its critical points can be surprisely considered scale invariant. Moreover, it is known that the curves describing the boundaries of the spin islands in a 2D-Ising model near to its critical point benefit from fractal properties.
Self-similar trajectories can also arise from stochastic processes. In particular, by studying how the fluctuations in a stochastic process vary when the range is rescaled, Hurst obtained a relation between the correlation or autocorrelation function of a time series and the fractal dimension of the trajectory[7]:

$$\mathbf{E}\left[\frac{R(n)}{S(n)}\right] = Cn^H \qquad\qquad n \to \infty \tag{2.8}$$

where $R(n)$ is the range of the first n cumulative deviations from the mean, $S(n)$ is their standard deviation and C is a constant. H is called the Hurst exponent and if the time series is self-similar it's directly related to the fractal dimension: $\Delta = 2 - H$ with $H \in [0,1]$.
It is well known for this kind of critical processes a relation that binds the Hurst exponent and the decay exponent of the power spectral density function, that will tend asymptotically to a power law $S(f) \sim f^{-\beta}$ [8]:

$$H = \frac{\beta + 1}{2} \tag{2.9}$$

- If $H = \frac{1}{2}$ then $\beta = 0$, the power spectrum is flat and the fluctuations in the time series are uncorrelated;

- $H > \frac{1}{2}$ and $\beta > 0$, the power spectrum is decaying as a power law, the process is positively correlated;
- while for $H < \frac{1}{2}$ and $\beta < 0$ it's anti-correlated, this could suggest the presence of a peak in $S(f)$ (Figure 2.3)

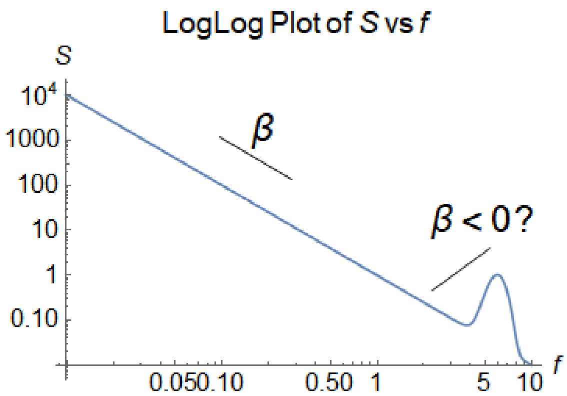

Figure 2.3: LogLog plot of $S(f)$. Minus the slope of a linear fit onto a specific region is the β that Hurst is estimating through relation (2.9)

It's hence undeniable the existence of a link between the decay rate of the correlations in a time series and the fractal dimension of the curve that stems from it.

2.6 Applications to cardiology and DFA

The Hurst exponent of the time series of RR intervals has been deeply studied[10]. Unfortunately, Hurst's estimator of H is susceptible to trends in the time series.
In order to better evaluate H in these cases a technique called *Detrended Fluctuation Analysis* (*DFA*) has been developed by Peng *et al.*[9]. Given a time series $\mathbf{X} = \{X_1, X_2, ..., X_N\}$ we first integrate it while subtracting its mean value:

$$y_i = \sum_{k=1}^{i} X_k - \langle X \rangle \tag{2.10}$$

Therefore the time series Y is divided in adjacent boxes of size n and within each one of these the *Root Mean Squared Error* is calculated by first subtracting a trend given by a fitted-polynomial $f^{l,n}$ of order l (Figure 2.4) and then averaging over all the boxes. This operation will be re-iterated for different box-sizes n giving birth to a function $F_l(n)$.

$$Y_k^{(l,n)} = \sum_{i=n(k-1)+1}^{kn} \left(y_i - f_{i,k}^{(l,n)} \right) \tag{2.11}$$

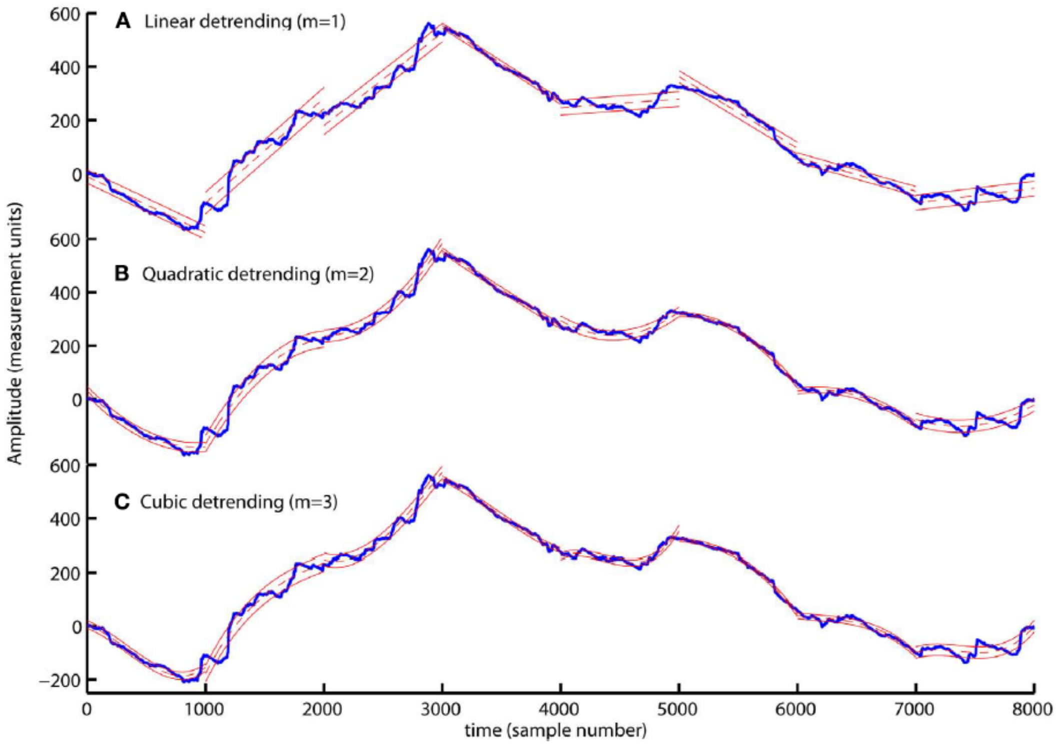

Figure 2.4: Detrending procedure in the DFA algorithm. Taken from [14]

$$F_l(n) = \sqrt{\frac{1}{N}\sum_{k=1}^{\lceil \frac{N}{n} \rceil} \left[Y_k^{(l,n)}\right]^2} \tag{2.12}$$

where k is a box index along the time series for a given box size n.
It is also interesting to observe how the fluctuation function is related to the autocorrelation function $R(t)$ of a discrete stochastic process [24]:

$$F_l^2(n) = \sigma^2 \left(L_l\,(0,n) + 2\sum_{t=1}^{n-1} R\,(t)\,L_l\,(t,n) \right) \tag{2.13}$$

where σ is the variance of the time series and $L_l(t,n)$ is a kernel that annihilates polynomial trends of order $l-1$.
If the process is scale invariant then:

$$F_l(n) \propto n^H \tag{2.14}$$

that is equivalent to say that if in log-log scale F_l scales linearly with respect to n, it means that the fluctuations vary as a power law under rescaling. The slope of that line will give the Hurst exponent H of the detrended time series. When we are fitting a polynomial of

order l we will say that we are using *DFA-l*.
We expect from the AR analysis illustrated in the previous section a spectral density that is not properly decaying as a power-law, but with some peaks emerging from it in the high frequencies range. This implies that the underlying process is not globally self-similar and a reckless application of the method could lead to false results. However, if the log-log plot of the function $F(n)$ preserves a piece-wise linear behaviour in some sufficiently extended region, one could define a different local scaling exponent α that instead of H, is not a global property of the time series.

Remark 4 *If the physiologic rhythms are characterized by oscillations with small periods T_k, we expect a different α for the linear behaviour of* $\log - \log F(n)$ *with a crossover between different regimes at $n \approx T_k$.*

The results of the application of *DFA-1* to the intra heartbeats time series showed a multifractal behaviour of the underlying process. In particular Golderberger et al.[10][5] analyzed data recorded during a 24h period on healthy young subjects, healthy elder subjects and on patients with cardiac problems incline to heart-failure. For the first group an exponent $H = 1$ was measured at all scales, for the second group a deviation of $H \approx 1.5$ was computed at very short scales ($n = 4, ..., 32$), while $H = 1$ but with a lot of fluctations (sign of multifractality) was recorded at very long scales ($n > 100$). For the group of patients with severe heart failure $H = \frac{1}{2}$ was computed for scales in the range $n = [4,16]$ and $H \approx 1.5$ for scales of size $n > 200$. We must beforehand specify that H should assume a value comprised in the interval [0,1] for an infinitely long time series in order for the relation $H \to \Delta$ to hold. If our time series is not long enough the previous relation does not always hold and H can assume also values outside of this interval. In particular it has been proved by numerical simulations that $H = 1.5$ describes the decay of autocorrelations in a Brownian exploding (correlated) motion. The latter results suggest that illness is the consequence of a loss of adaptability of the heart.
In healthy young subjects $H = 1$ points out the *sane* rate of decay of the autocorrelations in heart beats. In healthy elderly subjects the autocorrelations decay slower than normal at short scales and in a diverse fashion with respect to the normality also at very long scales. In patients incline to severe heart failure the heartbeats act as if they were completely uncorrelated at very short scales and strongly correlated at very large scales (Figure 2.5). It looks clear that loss of adaptability is a sign of deviation from sanity. Moreover, the fact that there is a huge amount of fluctuations in the intra-beats time series of healthy individuals at rest shed light on the well diffused biological concept of *homeostasis*. A sane individual is not one who can keep his current status fixed, but one who can efficiently adapt to any internal or external stimuli.

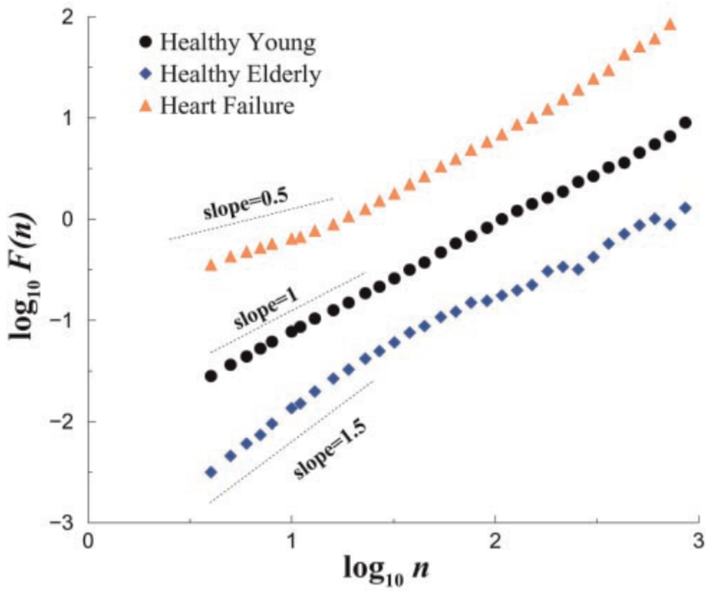

Figure 2.5: "Scaling analysis of heartbeat time series in health, aging, and disease. Plot of log F(n) vs. log n for data from a healthy young adult, a healthy elderly subject, and a subject with congestive heart failure. Compared with the healthy young subject, the heart failure and healthy elderly subjects show alterations in both short and longer range correlation properties. To facilitate assessment of these scaling differences, the plots are vertically offset from each other." Taken from [5]

.

Chapter 3

Heart Rate Variability during exercise

Hand in hand with technological development more and more fine and portable devices measuring echocardiograms became available. Therefore the immediate next step of the research in this field was dedicated to the study of the behaviour of the correlations in the time series of intra-beats intervals in groups of people that are exercising. More specifically, data of running athletes were collected and analyzed. Running usually requires an average heart-rate that can go from 100 bpm up to, usually, 180 bpm. (Figure 3.1)
The data used in this section were recorded using a Polar$_{®}$ H10 strap.

3.1 Limitations of DFA

From a first naive application of *DFA-1* it appeared as if in running subjects the short time scales fluctuations with $n \in [4,16]$ showed different type of exponents ranging from an anti-correlated to a strongly correlated regime depending on the instantaneous heart rate, while the ones with $n > 16$ were almost always the very typical ones of a correlated underlying stochastic process.
In contrast to the time series of subjects at rest, the outcomes of *DFA-1* on time series of exercises looks very different from one another. Varying the average and the instantaneous heart rate, the duration of the exercise and its type (normal running, sprints etc.) can tremendously affect the results of *DFA-1*. We hence wondered if *DFA-1* is a robust way of measuring H also on this data set.
One of the main differences of time series of exercises with respect to the ones of people at rest is their duration. For the latter the analysis performed by Golderberg et al. used a data set in which the measures were taken in a $\approx$ 24h period with very small perturbations in the average heart rate. The subjects were doing nothing, or at least they carried out activities that required a very small effort. On the contrary, time series of exercises can

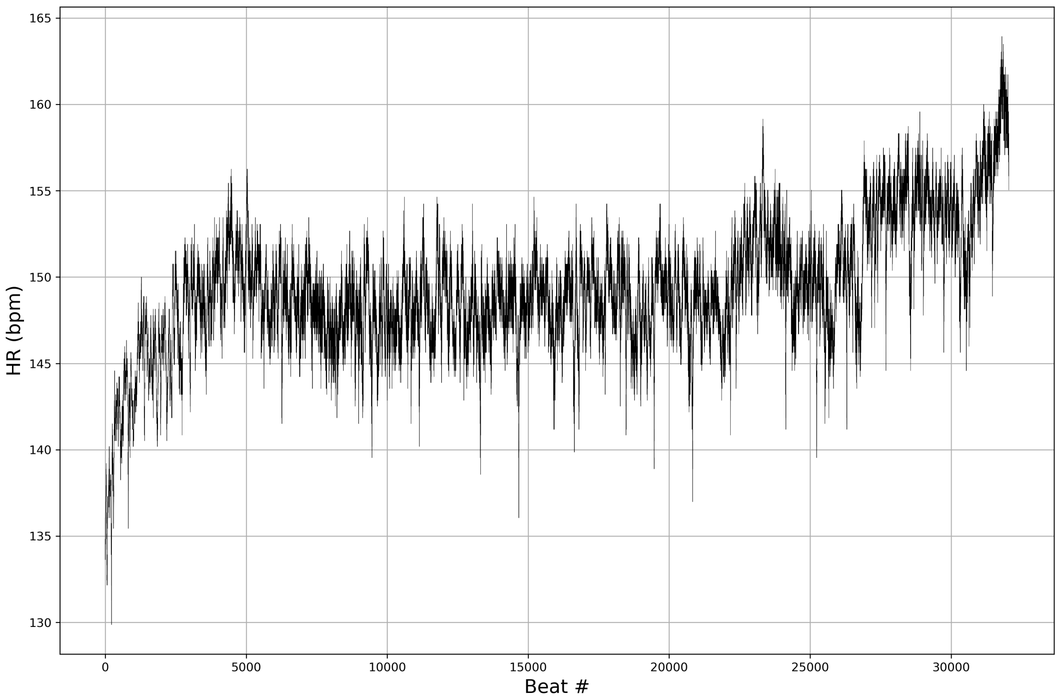

Figure 3.1: HR time series of a marathon run.

last from about 10 minutes to a couple of hours. The on-set of the physical activity is characterized by an exponential acceleration of the heart rate as it has also been shown by Javorka et al.[15]. Moreover, usually linear and/or periodic trends of relevant amplitude are also present. While *DFA-1* managed to efficiently detrend the long time series of resting subjects, this seems not to be the case for running time series.

3.1.1 The range of validity of DFA and local DFA

In order to be able to tell if DFA-1 is performing well on the new data set we first had to study how it behaves when analyzing simple time series.
In two papers Stanley *et al.* studied and analytically and via numerical simulations the performance of *DFA-1* on monofractal time series coupled with different trends[11] (linear, quadratic, power law -like and periodic) and mixed with several kind of non-stationarities[12] (segments deleted in the signal, uncorrelated spikes, segments of increments extracted by distribution with different variance, segments extracted by evolving distributions with different autocorrelations).
In particular, they analytically derived that for any order of *DFA* if the fluctuations are coupled with an uncorrelated trend, then the function $F_l(n)$ obtained by the application of *DFA* on the total time series will benefit of a sort of superposition principle of what

would have been the results of *DFA* applied only to the noise and only to the trend:

$$F_l^2(n) = F_{l,noise}^2(n) + F_{l,trend}^2(n) \tag{3.1}$$

They also analytically proved that in order to detrend any series affected by a polynomial trend of order m or by an exponential trend with exponent λ it is required to apply *DFA-l* with respectively $l > m$ and $l \geq 1 + \lambda$. This is a clear consequence of the fact that at the first step of *DFA* the time series is being integrated, and with it also its inner trend.
When *DFA-1* is performed on a linear trend, $F_{1,Ltrend}(n)$ is independent of the length of time series, but it grows as $\sim An^{\alpha_L}$ where A is the slope of the linear trend and $\alpha_L = 2$. Since it is well known that for a monofractal noise $F_{1,noise} \sim n^{\alpha}$, the total F in a log-log scale will appear as two piecewise lines with slope α and α_L and a crossover n_X.(Figure 3.2)
The F of a quadratic trend will also increase linearly with the length of the time series

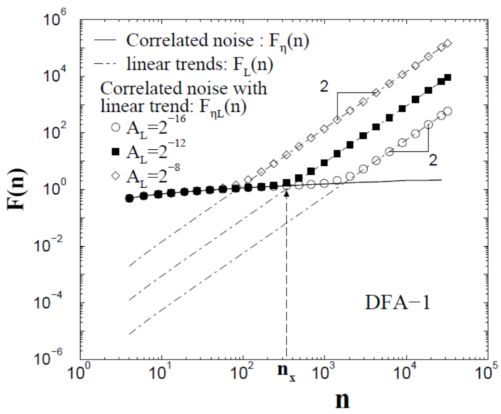

(a) "Crossover behavior of the root mean square fluctuation function $F \approx L(n)$ for noise (of length $N_{\max}2^{17}$ and correlation exponent $\alpha = 0.1$) with superposed linear trends of slope $A_L = 2^{-16}$, 2^{-12}, 2^{-8}. For comparison, we show $F_\eta(n)$ for the noise (thick solid line) and $F_L(n)$ for the linear trends (dot-dashed line). The results show that a crossover at a scale n_x for $F_{\eta L}(n)$. For $n < n_x$, the noise dominates and $F_\eta L(n) \approx F_\eta(n)$. For $n > n_x$, the linear trend dominates and $F_{\eta L}(n) \approx F_L(n)$." Taken from [11]

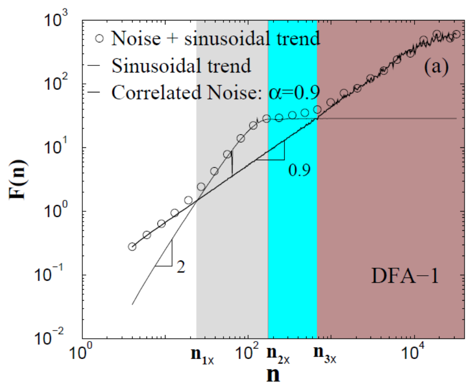

(b) "Crossover behavior of the root mean square fluctuation function $F_{\eta S}(n)$ (circles) for correlated noise (of length $N_{\max} = 2^{17}$) with a superposed sinusoidal function characterized by period $T = 128$ and amplitude $A_S = 2$. The rms fluctuation function $F_\eta(n)$ for noise (thick line) and $F_S(n)$ for the sinusoidal trend (thin line) are shown for comparison." Taken from [11]

Figure 3.2: a) DFA of linear trend b) DFA of sinusoidal trend

and this corresponds to a vertical upwards shift in the log-log plot.
The behaviour of *DFA-1* on periodic trends is instead quite peculiar. For a pure sinusoidal trend the F doesn't almost scale at all with the length of time series, for small scales n it grows as $F_{1,sin}(n) \sim \frac{A_S}{T} n^{\alpha_S}$ where A_S is the amplitude of the sin, T its period and $\alpha_S = 2$,

while for large scales it saturates to $F_{1,sin}(n) \sim A_S T$. Therefore, using the superposition principle, it is straightforward to remark that depending on the values of A_S, T and α one could notice 4 different regions in the log-log plot of F vs n with 3 crossovers (Figure 3.2). A first regime where F_{noise} is relevant up to the crossover n_{1x} with a second regime at small scales where $F_{1,sin}$ dominates, then it reaches the plateau at $n_{2x} \approx T$ and at n_{3x} F_{noise} becomes the leading one again. Increasing the order l of *DFA* both increases by 1 α_S and both shifts n_{1x} to higher scales, (always less than n_{2x}).
Regarding the non-stationarities, segment deletion on time series with fluctuations scaling as $\alpha > 0.5$ is not relevant, while if $\alpha < 0.5$ then, proportionally to the fraction of the data that was cut out, there will be a crossover dividing a regime at small scales where α dominates and another one at large scales where a slope of $\alpha_c = 0.5$ will be the leading one (Figure 3.3).
Instead, if uncorrelated random spikes are present in the signal, $\alpha_{spike} = 0.5$ will dominate over the noise at small scales for correlated time series and at large scales for anti-correlated ones (Figure 3.4).
The last two phenomena are very important since usually the recorded data present a lot of measurement artifacts that are almost always the aftermath of a skipped-beat (that will result as a spike since skipping a beat will double the intra-beats interval for that given value) or more rarely a RP-PR sequence mistaken for RR-RR intervals that will result in two opposite directed spikes (a shorter spike followed by a longer one). Before the analysis the raw data undergo a filtering process for artifacts. In our later studies we will delete all the intervals that will present values detected as outliers by a properly tuned rolling median filter. We prefer to delete the artifacts and not to keep them because, as it has been stated above, deleting the outliers should at least clean the F with correlated noise time series, and at the same time should also clean the ones with anti-correlated signals at small scales. All of the previous and also of the following results are obtained thanks to the superposition principle substituting each time the different part of the signal with one with all zeros.
For signals with same local α but different local variance it has been shown that the outcome *DFA* is greatly affected only if $\alpha < 0.5$ with a crossover at large scales with a region where $\alpha_\sigma = 0.5$.
While for signals with different local α we can appreciate a crossover at a scale n_x only if the biggest part of the time series is composed by data characterized by $\alpha < 0.5$. It is impressive to remark that even if there is a time series formed for the 90% by $\alpha = 0.1$ and for the remaining 10% by segments with $\alpha = 0.9$, the total F will be almost immediately dominated by the correlated signal starting at $n \approx 16$ (Figure 3.5)
We should also say that, as pointed out in reference [13], every *DFA-l* has an optimal range of validity, with a lower n_{min} that increases the higher is the order of l because we will need more points to fit the the trend in each box along the time series, while attempting to avoid the risk to overfit. And more generally, *DFA* tends to overestimate the evaluated H for noises with $\alpha < 0.5$ and $\alpha > 1$.

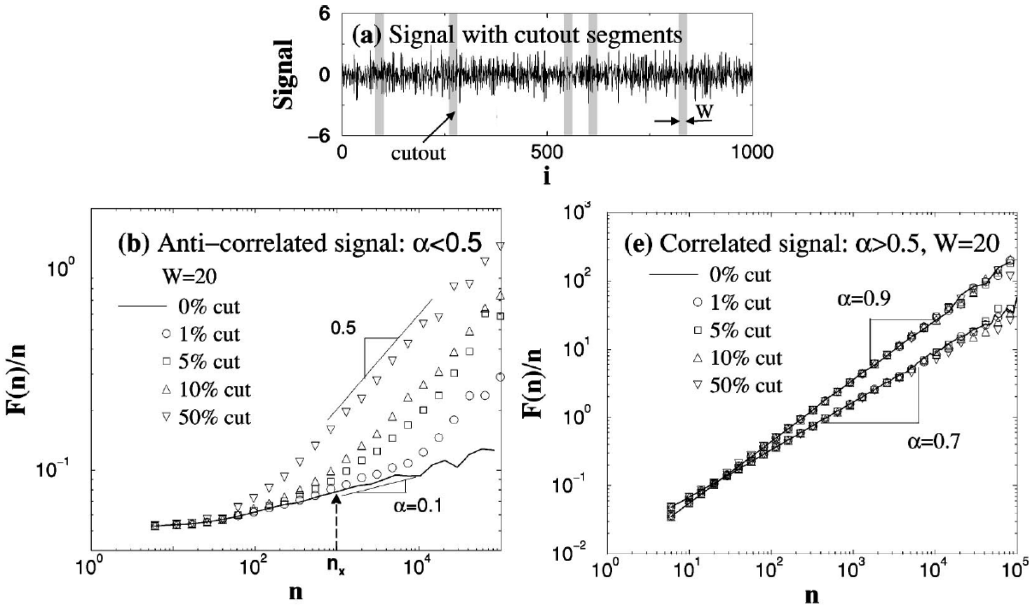

Figure 3.3: "Effects of the ''cutting'' procedure on the scaling behavior of stationary correlated signals. $N_{\max} = 2^{20}$ is the number of points in the signals (standard deviation $\sigma = 1$) and W is the size of the cut out segments. (a) A stationary signal with 10% of the points removed. The removed parts are presented by shaded segments of size $W = 20$ and the remaining parts are stitched together. (b) Scaling behavior of nonstationary signals obtained from an anticorrelated stationary signal (scaling exponent $\alpha < 0.5$) after the cutting procedure. A crossover from anticorrelated to uncorrelated ($a = 0.5$) behavior appears at scale n_x . The crossover scale n_x decreases by increasing the fraction of points removed from the signal. We determine n_x based on the difference Δ between the logarithm of $\frac{F(n)}{l}n$ for the original stationary anticorrelated signal ($\alpha = 0.1$) and the nonstationary signal with cut out segments: n_x is the scale at which $\Delta > 0.04$. (e) Cutting procedure applied to correlated signals ($\alpha > 0.5$). In contrast to (b), no discernible effect on the scaling behavior is observed for different values of the scaling exponent α, even when up to 50% of the points in the signals are removed." Taken from [12]

Remark 5 *Keeping all of these results in mind, it is now evident that, for a preprocessed artifact-free time series of RR intervals of running persons, if we want to analyze when and how the fluctuations switch from a correlated to an anticorrelated regime it is mandatory to focus on extremely short scales with* $n \rightarrow\sim 16$*.*

This now justified assumption is in agreement with what was noticed naively using a *dynamical* modified version of the *DFA-1* algorithm that serves to measure the *local Hurst exponent* in a interval of fixed size W around any entry of the time series. This procedure not only allows us to infer the local properties of the time series, but collecting all the computed instantaneous local Hurst exponents H_t we are able to build up a statistics for

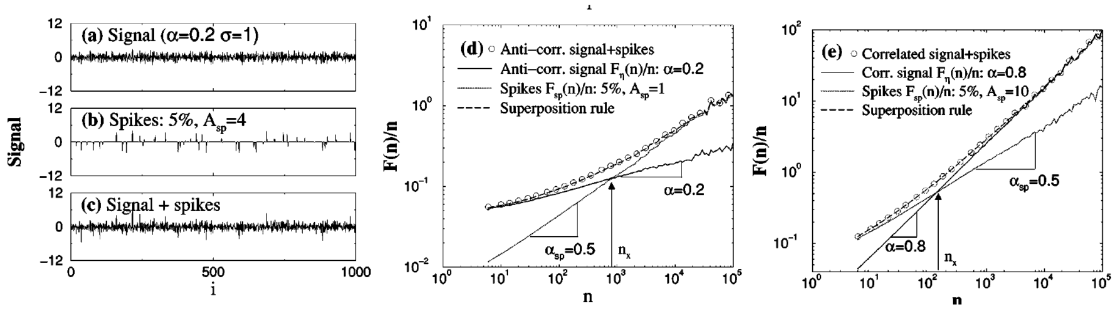

Figure 3.4: "Effects of random spikes on the scaling behavior of stationary correlated signals." Taken from [12]

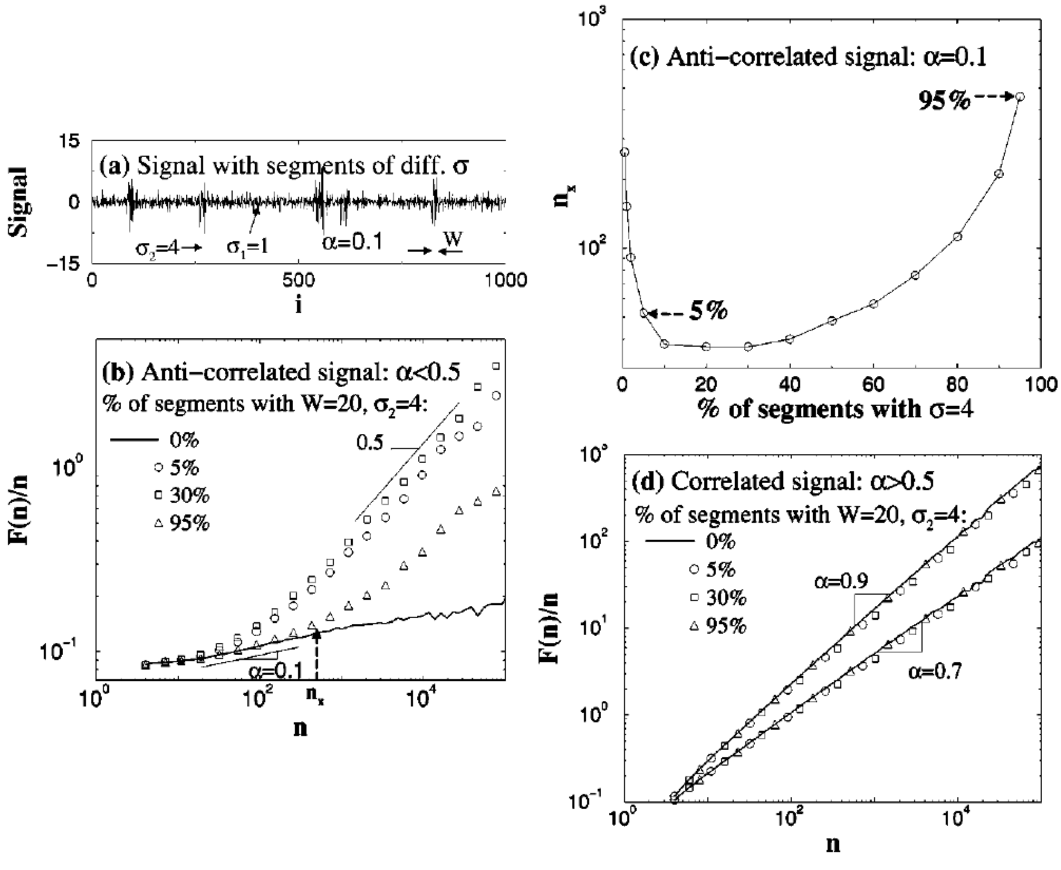

Figure 3.5: "Scaling behavior of nonstationary correlated signals with different local standard deviations." Taken from [12]

its distribution that will be characteristic of a multifractal behaviour.
The algorithm works as follow: first we choose an observation window size W within the time series, then for every entry starting from the one of index $\frac{W}{2}$ to the one of index

$N - \frac{W}{2}$ we compute *DFA-1*. As Kantelhardt recommends we should select a W that is at least 4 times the value of the maximum scale for which *DFA* is computed[16]. In order to obtain a smoother time series of H_t we may subdivide the observation window, during the evaluation of the RMS, in many n sized overlapping boxes shifted by 1 step instead of $\frac{W}{n}$ adjacent non overlapping boxes. This will not affect mean value of H_t over the whole series but will drastically reduce its local spread.
While on the long series of patients at rest we had at most a constant trend and hence *DFA-1* was enough to contrast, on average, all the perturbations, we might need a higher *DFA* order to detrend the new data-set in an acceptable fashion. Additionally, since the most frequent kind of trend in our data set is the exponential one, it goes without saying that we should procede analyzing analytically what happens when we are facing one of this sort with *DFA*.

3.1.2 The effects of an exponential trend

Let's consider an exponential trend of the form

$$X_i = H_{min} + A\left(1 - e^{-\frac{i}{\tau}}\right) \tag{3.2}$$

The first step of *DFA* consists in integrating the time series. We will skip the subtraction of its average value since it will be a constant that will just change the value of H_{min}. Moreover, since any constant trend is perfectly removed by *DFA-1* we can put $H_{min} \equiv 0$ without loss of generality. Therefore

$$y_i = A\sum_{k=1}^{i}\left(1 - e^{-\frac{k}{\tau}}\right) = A\left(\frac{1}{1-\gamma} + k - \frac{\gamma^{-k}}{1-\gamma}\right) \tag{3.3}$$

where, for simplicity of notation, $\gamma \equiv e^{\frac{1}{\tau}}$. We want to compute, according to (3),

$$Y_k^{(1,n)} = \sum_{i=n(k-1)+1}^{kn}\left(y_i - f_{i,k}^{(1,n)}\right) \tag{3.4}$$

$$f_{i,k}^{(1,n)} = a_0^{(k,n)} + a_1^{(k,n)} i \tag{3.5}$$

the latter is the best linear fit of the succession y in a box of index k and size n obtained with least squares regression.
Now it's the time for a small remark:

Remark 6 *We notice that detrending in this way corresponds to subtracting the polynomial that minimizes the fluctuations (the square of Y) in each box. This will be always the case if the noise is extracted by a symmetric thin-tailed distribution, otherwise we might consider as a trend what really is an extremed valued fluctuation. Anyway in the next step the averaging over all Y for a given n will mitigate the effect.*

Therefore proceding with the minimization problem following the scheme of Stanley *et al.*[12] we obtain:

$$\frac{\partial Y_k^2}{\partial a_m^{(k,n)}} = 0 \qquad \forall m = 0,1 \tag{3.6}$$

and hence a system of 2 equations in the unknowns $a_m^{(k,n)}$

$$y^{(m,k,n)} = a_0^{(k,n)} t_{m,0}^{(k,n)} + a_1^{(k,n)} t_{m,1}^{(k,n)} \tag{3.7}$$

where

$$y^{(m,k,n)} = \sum_{i=n(k-1)+1}^{kn} y_i i^m \tag{3.8}$$

and

$$t_{m,j}^{(k,n)} = \sum_{i=n(k-1)+1}^{kn} i^{m+j} \qquad \forall j = 0,1 \tag{3.9}$$

From which we recover first $a_m^{(k,n)}$, then Y_k^2 and finally a very long complicated expression for $F(n)$ that for large enough scales n saturates to

$$\lim_{n\to\infty} F(n) \sim A\sqrt{\left(\frac{1-\gamma^{-2N}}{N}\right)} \tag{3.10}$$

We notice that the amplitude A just causes a vertical shift in the loglog scale plot.
This behavior is similar to the one obtained for the periodic trend, with the exception that luckily for the exponential trend the effect decreases with an increasing N. For long time series the superposition principle will allow the fluctuation function of the noise to eventually overcome the one of the exponential trend. For short time series this is unlikely to happen and the trend may be dominating.

Before starting to look for a robust technique that could serve for the massive analysis of all running time series we have to check that the trends and the noises are uncorrelated. This is equivalent to checking the validity of the superposition principle on real data. In order to do so we first generate an exponential time series, then we add a noise to it, afterwards we numerically compute the F_E of the trend with the obtained parameters, subsequently we assume that the noise has approximately a monofractal behaviour, hence we perform *DFA-1* on the time series and subtract from it the F computed before for the trend. From *DFA-1* we noticed that the F first logarithmically scales with exponent H and then it bends to another α_E before turning to a plateau. There is almost a perfect overlap between F_{total} and F_E after the first turn. Therefore we subtract F_E from F_{total} and if the remaining F will preserve the same linear slope both for small and big scales we can conclude the validity of the superposition principle. As we notice from the plots in Figure 3.6 on the time series analyzed the superposition principle is valid, therefore we conclude that the noise and the exponential trends are uncorrelated.

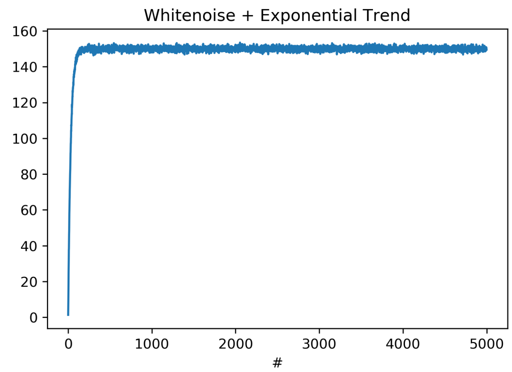

(a) Example: Time series with $N = 5000$ built by summing an exponential trend of the form: $u_i = 150\left(1 - e^{-\frac{i}{30}}\right)$ and a white noise $X_i \sim \mathcal{N}(0,1)$.

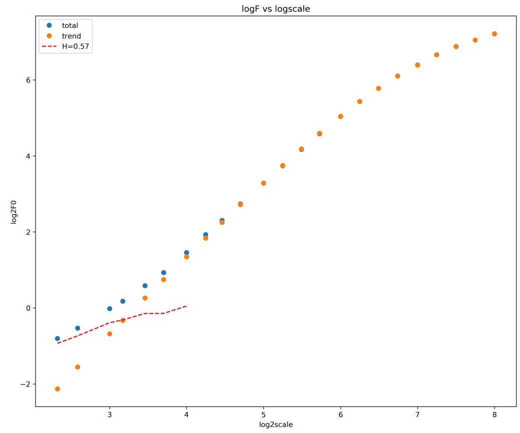

(b) Log-log plot of $F(n)$ obtained with *DFA-1* both on the whole time series of Figure **??** and on the trend alone. Using the the superposition principle we can derive the quantity $F_{noise}(n) = \sqrt{F^2(n) - F^2_{trend}(n)}$. Its slope is $H \approx 0.57$ as expected.

Figure 3.6: a) Example of generated exponential trend b) DFA of the signal in a)

3.2 Applications of DFA to real data

Now we can proceed estimating the time series H_t for a time series that has some evident exponential trends (Figure 4.2) with $n_{min} = 5$, $n_{max} = 16$ and $W = 80$. The selected time series also has some artifacts left. This is a nice study-case to practically show how artifacts can influence the outcome of DFA.
We notice from (Figure 3.8) that also H_t exhibits an exponential trend, and this is due to the fact that, even though we are at very small scales n, we are not efficiently detrending. Moreover, as expected from the setup, since we are assigning the value H_t to every entry t performing DFA in an interval of size W around it, the information about drastic changes in the time series at an instant t^* are visible starting from $H_{t^*-\frac{W}{2}}$ up to $H_{t^*+\frac{W}{2}}$. Around the spiky artifacts we notice a small increase of H_t towards an uncorrelated behaviour. When the obeservation window meets the sudden relaxation and then the start of the exponential rise, H_t becomes instantaneously > 1.
We therefore perform *DFA-2* with the same values as before but $n_{\text{min}} = 6$ in order to avoid unstabilities due to overfitting. Moreover, we will adoperate an extra trick: since we are and expecting a crossover to another α behaviour at scales $n \approx 16$ (that can differ a bit for each subtimeseries) and imagining that *DFA-2* for small $n \approx 6$ can be unstable, and since in addition to that we have only very few points in our loglog plot, we compute the slope of the linear fit (H_t) using the Theil-Sein estimator for the best median-linear fit. This approach is much more robust because it is more stable with respect to the presence of

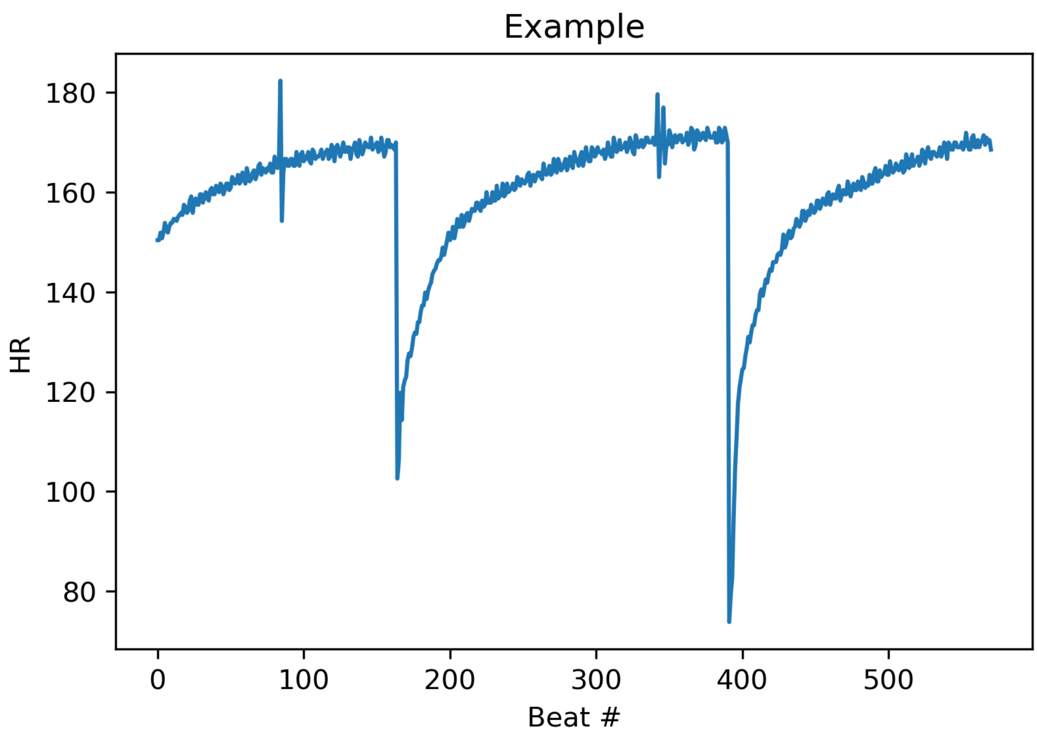

Figure 3.7: Example: Values of heart rates along a running time series. Three approximately equal exponential trends and some artifacts are present.

outliers that could arise from the presence of fluctuations with a different local α (at big n) or due to overfitting (at small n). It's remarkable how in (Figure 3.9) the exponential trends are greatly suppressed. This is accountable not only to the fact that the linear part of the exponential trend is perfectly filtered out, but also the first crossover n_{1x} is shifted to a larger value.
Quite strangely, there are many instants for which H_t assumes values < 0 or > 1. These effects are due to the unstabilities of *DFA-2*, to imperfections in detrending, to the small dimension of the observation window W and to the small scales n taken in account. In order to limit the presence of isolated negative or positive spikes in H_t, and also not to overestimate too much the exponents for $\alpha > 1$, we developed a modified version of *DFA* that we baptized as *medianDFA*. The only adjustment consists in replacing the estimator of the average value of the RMS's Y^2 with their *median*.

$$F_l(n) = \sqrt{median\left[Y^{(l,n)2}\right]} \tag{3.11}$$

In this way if in some boxes we happen or to be overfitting or to be sampling from the distribution with a much higher α, if we still have a decent set of values $Y^{(l,n)}$, the outliers will be reasonably ignored. On the contrary, the mean value computed as in normal DFA is

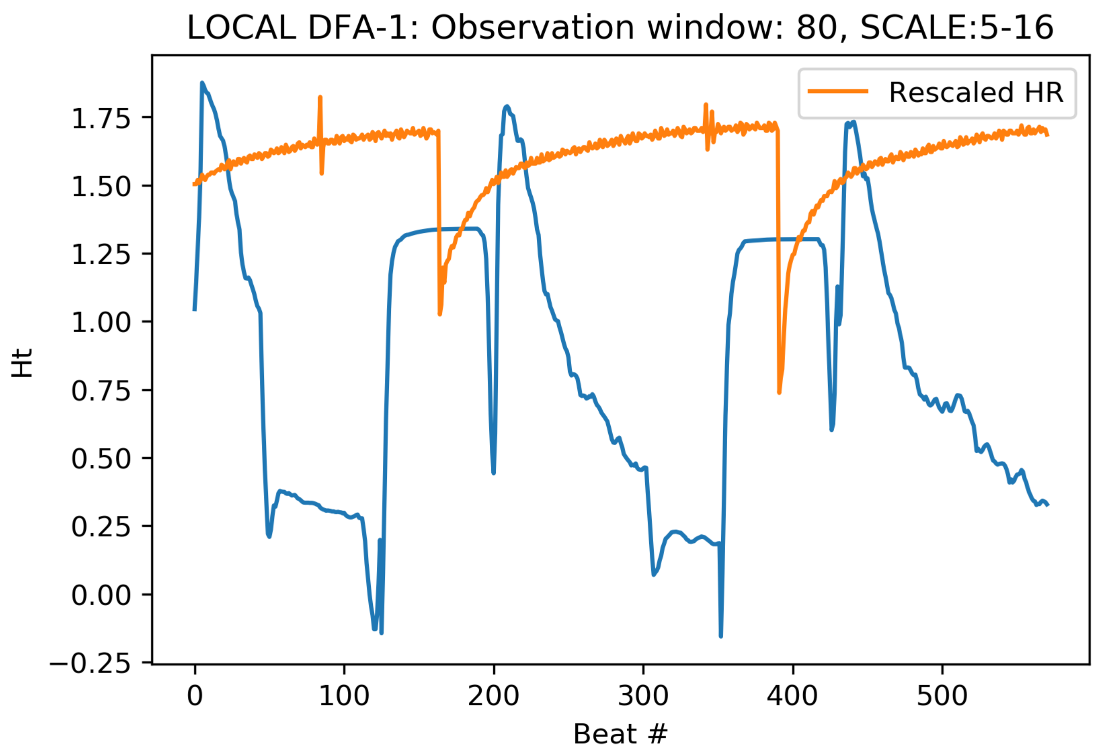

Figure 3.8: Local DFA-1 over the overlapped rescaled heart rates time series (the orange curve). Scales n ranging from 5 to 16, Observation window size: 80. The blue curve is the H_t time series.

consistently shifted by outliers. In (Figure 3.10) the series has lost some of its smoothness, but there are nor negative values nor values greater than 1.
In other examples there will still be present values of H_t larger than 1, but their maximum value with respect to normal *DFA-2* will be contained. It's important to state that the *median* is a linear operator only if acting on monotonic ordered (with the same ascending or descending order) list of values.
Nevertheless, the *median* and the *mean* estimator give almost the same result if we are sampling from a symmetric, single peaked distribution. Keeping this in mind, using the *median* on these ranges of n should only help to filter the outliers out the true results and sample H_t directly from the noise which scales with exponent α.
Therefore, we applied local DFA-1 and local DFA-2, in their normal and median versions, to 200 time series of several lengths. These time series do not contain only long runs, but also different kind of aerobic work-outs. The exercises were all performed by the same athlete, a young sane male. In order to deduce a relation between the scaling exponent H_t and the instantaneous Heart Rate, we divided the data in Heart Rate bins of size = 2.5 bpm . For each bin we will report the median value of H_t (since it's hugely fluctuating,

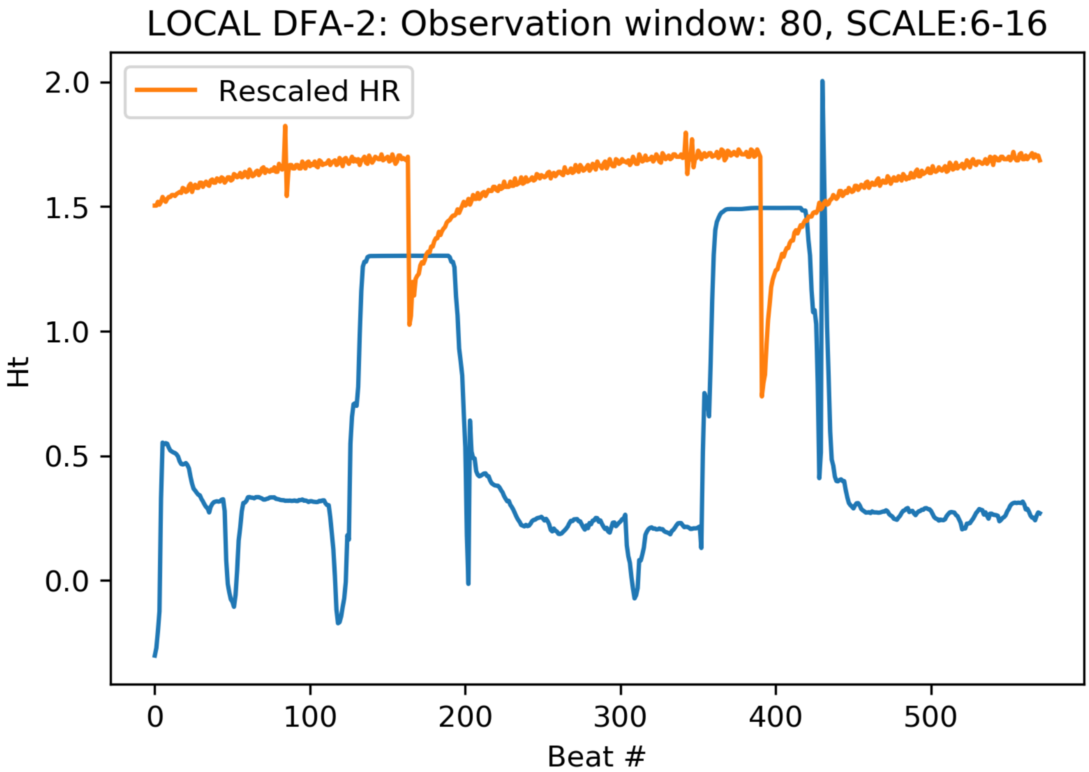

Figure 3.9: Local DFA-2 over the overlapped rescaled heart rates time series (the orange curve). Scales n ranging from 6 to 16, Observation window size: 80. The blue curve is the H_t time series.

this approach is less affected by outliers). We must not forget that the athlete is spending different amount of times with disparate Heart Rates. So it might be also useful to plot the histogram of the instantaneous Heart Rates on the whole dataset (Figures 3.11, 3.12).

From the bin statistics plot we notice that for ”low” exercising heart rates (up to 130 bpm) H_t starts being of order 1, then it decreases, approaching very rapidly < 0.5, suddenly it increases again showing a little bump with $H_t \approx 0.8$ around 160 bpm and finally returning to an anti-correlated regime (< 0.5).

For starters we hoped that the presence of this bump would be related to the onset of a new ventilatory regime. It’s known from physiology that at a given point, in order to compensate for the increase in effort, the ventriculi starts to open more, sucking in more blood and therefore increasing the flux that is being pumped out. If H_t told us something about the amount of stress that the heart is experiencing, this should have been the case. Unfortunately a closer analysis on the single time series showed that this effect is created by the trends. We can infer from the histogram (Figure 3.13) that the athlete is spending most of the time with an heart rate that is in the range just before the bump. This means that there are a lot of running time series were the heart is saturating, after an exponential

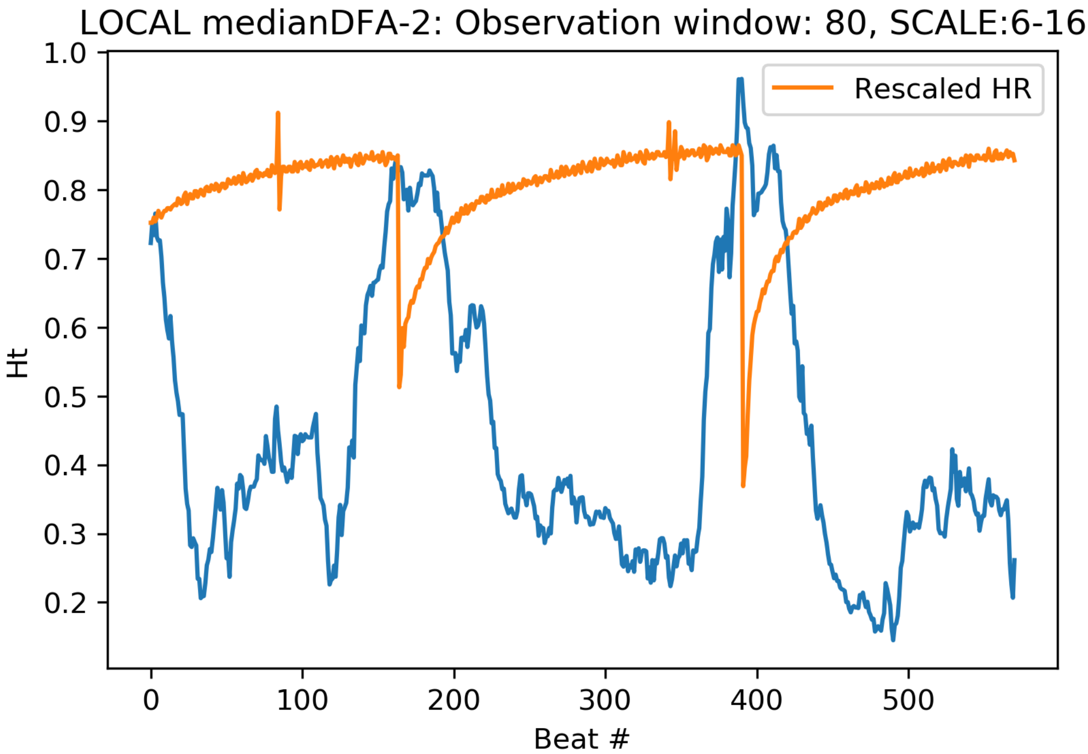

Figure 3.10: Local medianDFA-2 over the overlapped rescaled heart rates time series (the orange curve). Scales n ranging from 6 to 16, Observation window size: 80. The blue curve is the H_t time series.

acceleration, to a value comprised in that range. All the higher heart rates comes from a fewer amount of points, and in order to reach those rates the patient must accelerate more. With the aim of finding out if this effect is 1) common to every human being, 2) not caused by trends; we selected 40 short time series from another healthy patient, a middle-aged healthy male. These data are related to exponential accelerations from rest to a whole range of constant heart rates going from 140 bpm to 180 bpm. We notice from the bin statistics (Figure 3.14) that, overall, the behaviour of H_t with respect to the Heart Rate is the same. It starts from $H_t \approx 1$ and it becomes rapidly strongly anti-correlated, also now there is a bump, but its maximum is slightly less than 0.5. However the exponent is anti-correlated in the time series when the heart rate is saturating to a value that lies in the range of the local maximum. We can hence reasonably state this effect is generated by trends.

Remark 7 *The conclusion we can draw from DFA performed with boxes of size scaling from $n = 4$ to $n = 16$ is that during exercise the fluctuations in the Heart Rate are* anti-correlated.

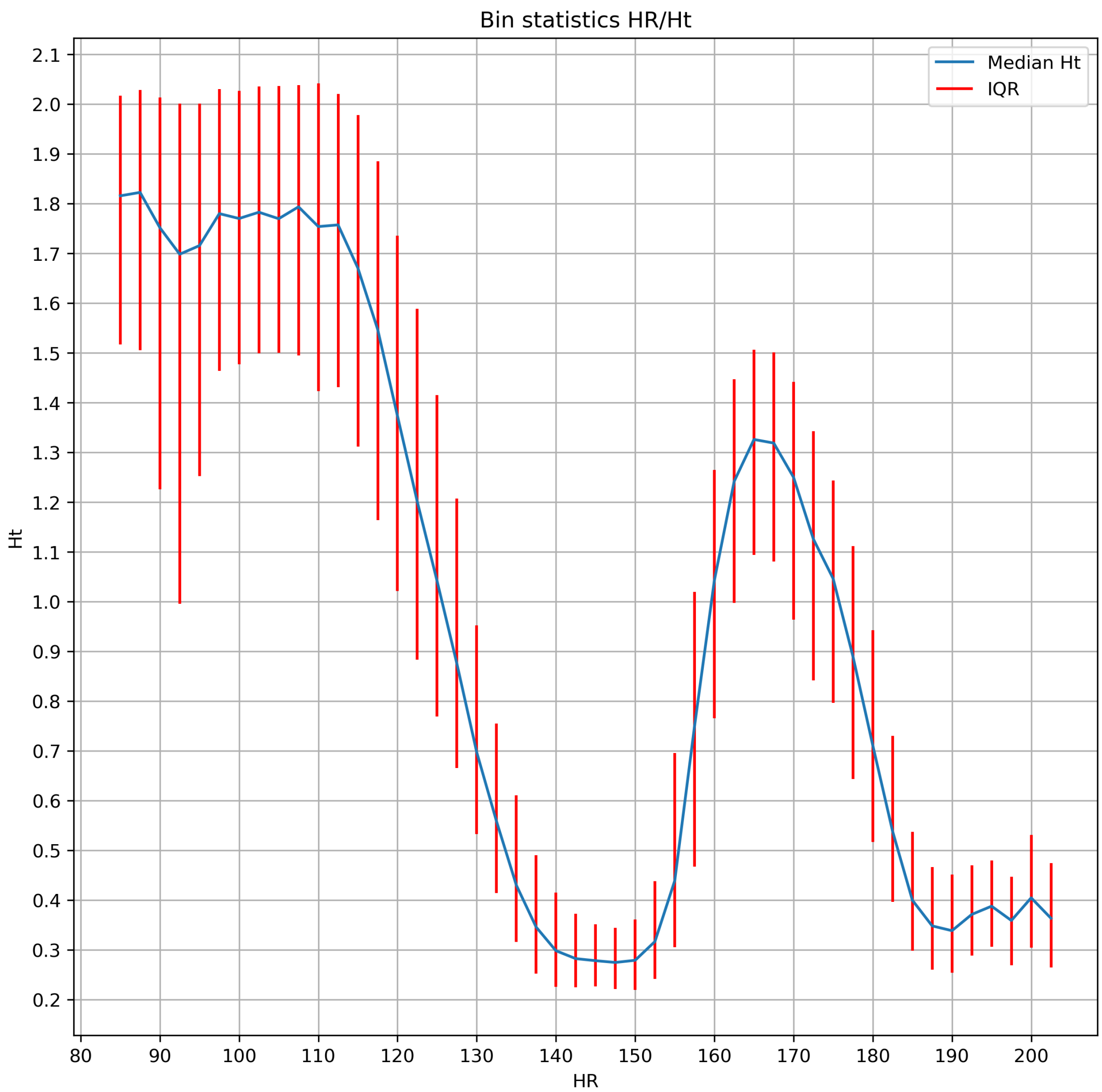

Figure 3.11: Bin statistics of H_t vs HR for DFA-1 over 200 time series. The blue curve are piecewise linear interpolation of the median value in the bin. The red segments represent the bin interquartile range.

3.3 (Partial) Autocorrelation Function and Lags

Let's now do a small recap: our goal is to study the Heart Rate Variability and to infer some parameter that will link the HRV to the status of the patient or to its current level of stress (if during exercise). A straightforward application of the Fourier Spectral Analysis is not possible, for the signal is non-linear, non-stationary and may also be short.
The first method we studied fitted an AR model and tried to perform Fourier Spectral Analysis upon it. The spectral density of the fitted AR model showed non negligible

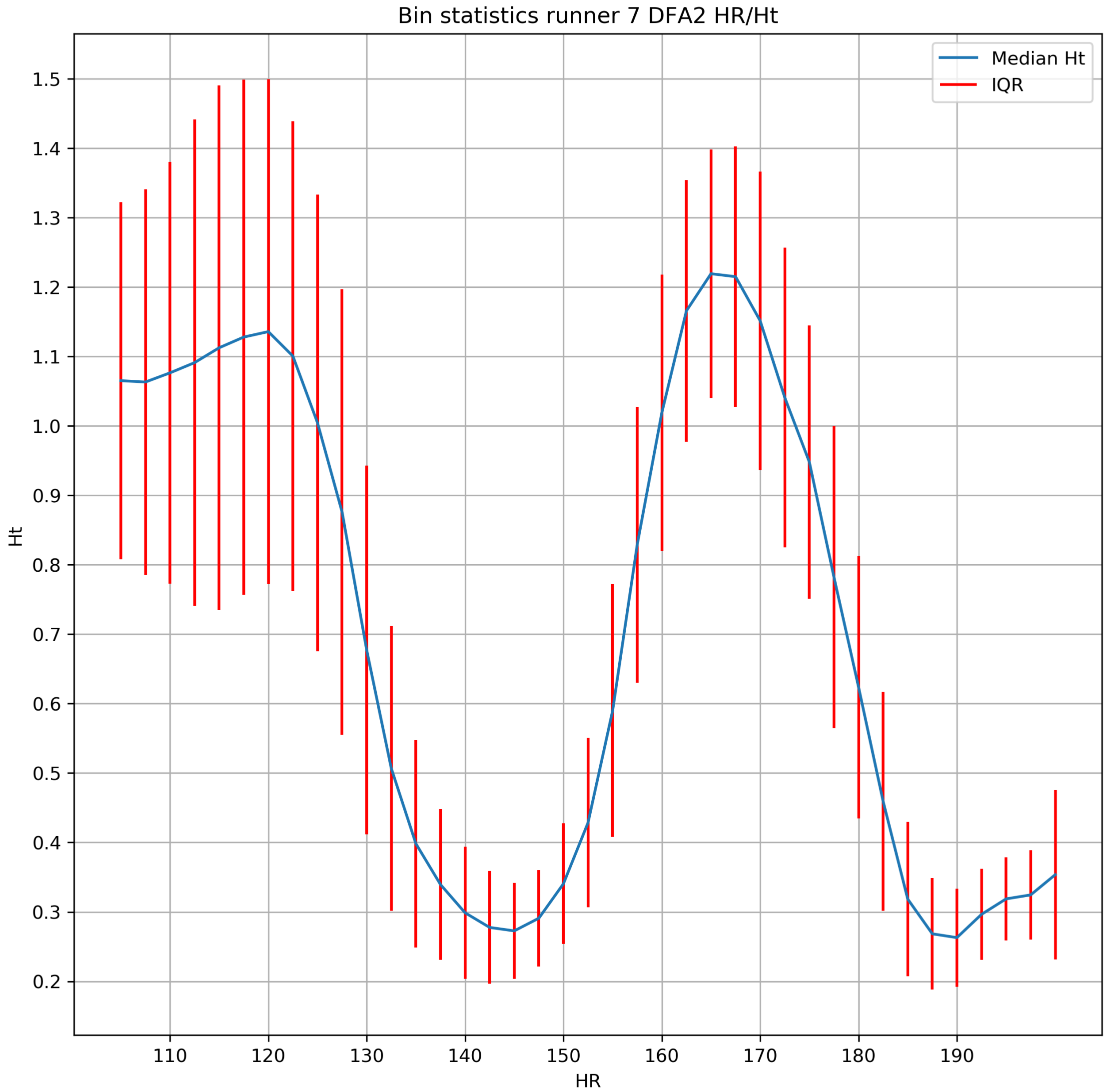

Figure 3.12: Bin statistics of H_t vs HR for DFA-2 over 200 time series. The blue curve are piecewise linear interpolation of the median value in the bin. The red segments represent the bin interquartile range.

peaks in a *high frequency* band with frequency $f > 0.1$ beats^{-1}. Heart Rate variability was pointed out by the ”normalized” variance of the residual time series, or better by the error in the fit.

The second method exploited an alleged scale invariance and an asymptotic relation between the fractal dimension of the trajectory (built up considering the time series as increments) and the decay exponent of its Fourier Spectral Density, although for short time series it is hard to evince if that relation really holds, or better if the autocorrelation function is decaying exponentially or as a power-law.

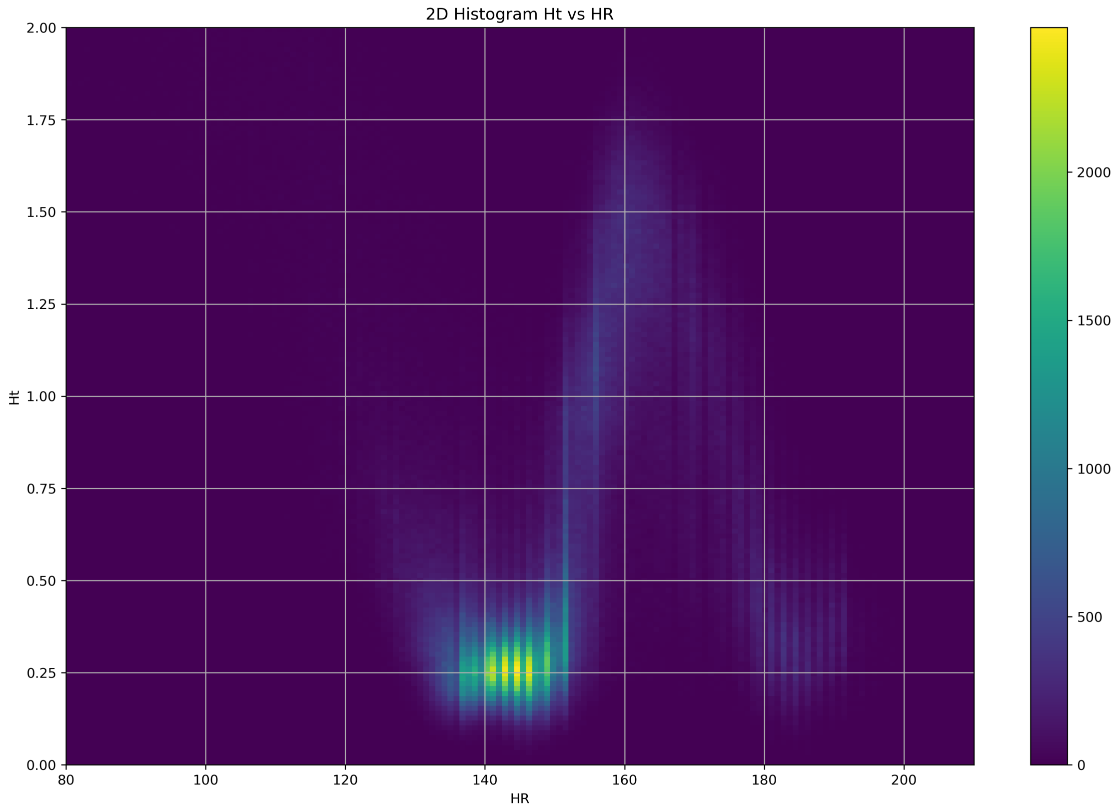

Figure 3.13: 2D Histogram of H_t computed with DFA-1 and HR. The color bar refers to the number of points in each bin.

Nevertheless, both techniques gave unsatisfactory quantitative results in the evaluation of a precise link between the HRV and the heart rate. On one hand the first method is way too approximative because during the process of fitting we are discarding too many important details; on the other also the second method is not correct due to the failure of scale-invariance.
We will try to entirely avoid the Fourier Spectral Analysis imagining that the RR time series can be described by an AR model coupled with some regulatory periodic physiologic mechanisms. Hence we will compute directly the discrete partial autocorrelation function (*ACF*) to obtain estimates both of the order of the AR model, both of the period of oscillations. This has not been originally done for the following list of reasons:

1. because of the trends, that have a great impact on the ACF and usually enforce correlations on every lag

2. if the original signal is periodic, the ACF won't decay but will also be a periodic function. If we want to evaluate the period without recurring to the Fourier Transform, we will have to compute the ACF for a number of lags such that will allow the

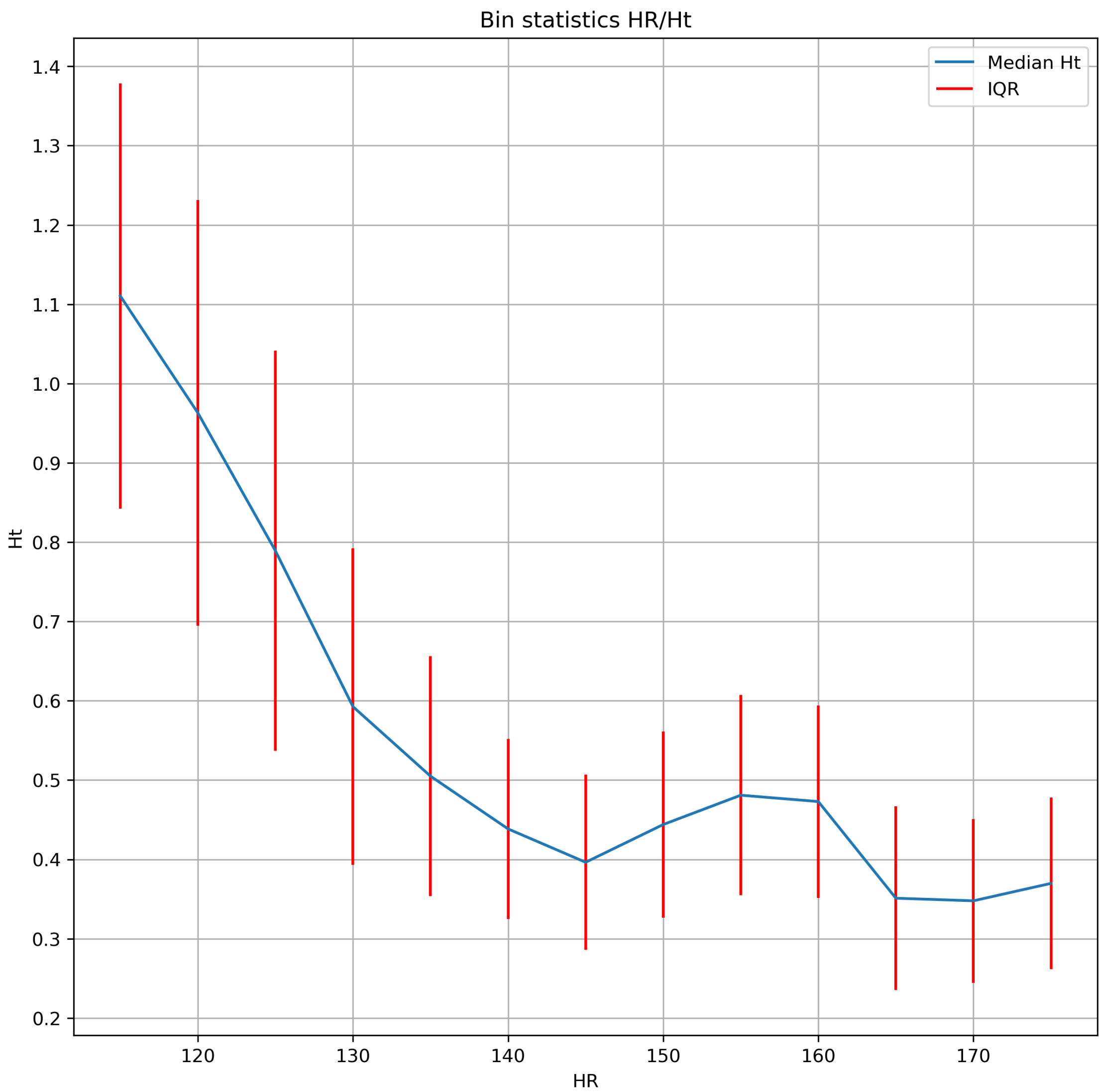

Figure 3.14: Bin statistics of H_t vs HR for DFA-2 over 40 intervals time series. The blue curve are piecewise linear interpolation of the median value in the bin. The red segments represent the bin interquartile range.

periodic pattern to repeat itself a sufficient amount of times. In order for the estimate to be statistically significant a large amount of points along the time series will be needed.

3. because, in principle, people were interested in the decay rate of the ACF at great distances/times and DFA was more convenient and numerically robust for short data sets [20]

3.3.1 The relation between DFA, an oscillating signal and an AR process

We will now try to understand how well an oscillatory signal can be modeled by an AR process and how these two are related to the fluctuation function computed with DFA. This research has been carried out by Meyer and Kantz in a recent paper[20] for AR(2) processes but we believe that could be, in further studies, generalized to high order ones. They define an AR(2) process:

$$X_t = a_1 X_{t-1} + a_2 X_{t-2} + \eta_t \tag{3.12}$$

a_i are the model parameters and η is any kind of uncorrelated noise. Being σ_η the variance of the noise, the variance of the whole process can be computed analytically and assumes the following form:

$$\sigma_X^2 = \frac{\left(1 - a_2\right) \sigma_\eta^2}{\left(1 + a_2\right)\left(1 - a_1 - a_2\right)\left(1 + a_1 - a_2\right)} \tag{3.13}$$

One can define a backshift operator B [18] to write (3.12) as

$$\left(1 - g_1 B\right)\left(1 - g_2 B\right) X_t = \eta_t \tag{3.14}$$

where g_i are complex roots. Using the Yule-Walker equations, one can calculate analytically the correlation function R:

$$R(t) = c_1 g_1^t + c_2 g_2^t \tag{3.15}$$

where c_i are constants, $R(1) = \frac{a_1}{1-a_2}$ and $R_0 = 1$.
Since $R(t)$ is the superposition of two AR(1) autocorrelation functions, the superposition principle extends to the DFA-1 fluctuation function, and using equation (2.13) and (3.1):

$$F^2(n) = \sigma^2 \left(c_1 F_{g_1}^2(n) + c_2 F_{g_2}^2(n) \right) \tag{3.16}$$

When $\Re(g_{1,2}) > 0$ the AR(2) process can be mapped into a discrete damped driven harmonic oscillator with period:

$$T = \frac{2\pi}{\arctan\left(\Im(g_1)/\Re(g_1)\right)} \tag{3.17}$$

The authors of the paper also noted how for large n equation (3.16) scales as $n^{\frac{1}{2}}$,as if the process were not correlated.

Remark 8 *If the superposition principle works also for higher order AR(p) processes, then all of them will scale for large n asymptotically with exponent $H = \frac{1}{2}$. So one could* *infer from the asymptotic trend of the fluctuation functions at large scales if the analyzed time series is generated by an autoregressive process. For small scales the behaviour of F is completely non trivial and non-linear. It's astonishing the conclusion that, even though the fluctuation function is not a power-law, we can still use DFA in a more general sense to extract important quantities about the behaviour of the correlations in the time series, and also the period of its dominant oscillation if there is one.*

Successively, Meyer and Kantz fitted not-damped oscillators like a pure sine-wave with an AR(2) process (Figure 3.15). They then approximately estimated the period and found out that for small scales the results are still *good*. Anyway, contrarily to the perfect sine-wave behaviour of Figure (3.2), the fluctuation function in (3.16) will behave according to the exponent $H = 0.5$ for large scales. Since, as will be reported in the next subsection,

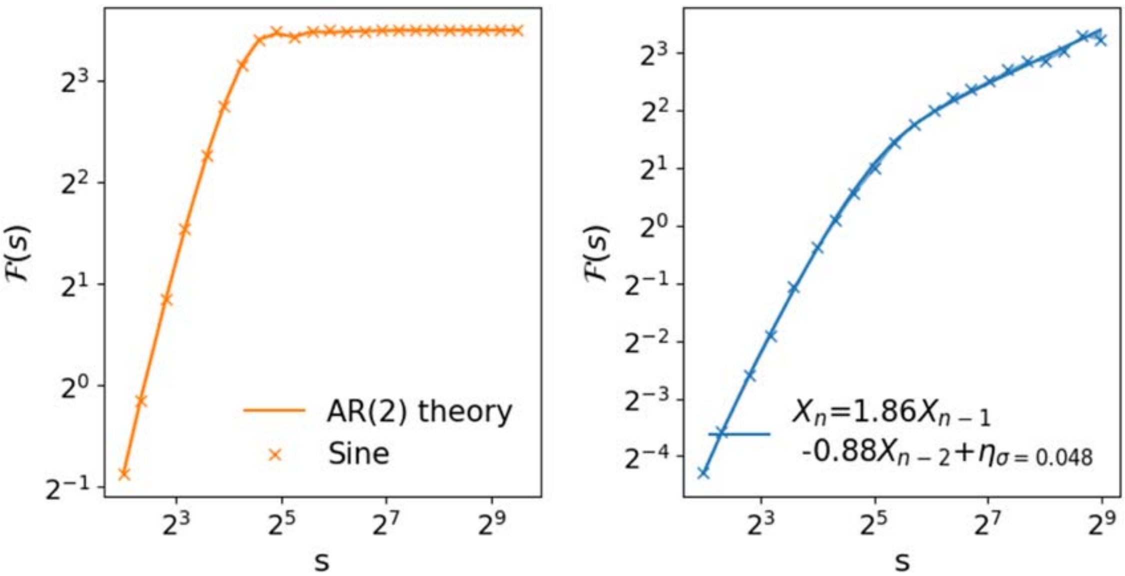

Figure 3.15: "LEFT: theoretical result of AR(2) fitted to the DFA-1 fluctuation function of a sinusoidal signal with length 3000 and period length $T = 20$. For 1000 realizations with random phase shifts (not in the picture) was fitted. The results $a_1 1.90256 \pm 0.00004$, $a_2 = -0.999997 \pm 0.000001$ and $T = 20.047 \pm 0.003$ indicate only a small bias, but even smaller variance. RIGHT: theoretical result of AR(2) fitted to the DFA-1 fluctuation function of the 11 month averaged ENSO time series (e.n.: that has period $T \approx 3.3y$). Here they obtain the period length $T = 39.6m = 3.3y$." Taken from [20]

there is a straightforward relation between the coefficients of an AR model and the partial autocorrelation function, and since, as we have just seen through, fitting an AR model for short time scales can give discretely accurate results for the period of dominant oscillating modes in the time series without recurring to Fourier Spectral Analysis, we will now compute directly the pACF on our data.

3.3.2 Local-pACF and applications

If the time series is wide-sense stationary and periodic, for example a pure sine wave, the ACF will be a cosine with the very same period. In order to visualize this behaviour in the estimation of the ACF that we perform, we should at least notice the same repeating pattern 2 or 3 times. If the period of the oscillation is $T = 10$, we would need to compute the value of the ACF for at least 30 lags. With the goal of obtaining a marker for the instantaneous HRV that varies with activity intensity, we should hence compute the ACF in a sliding moving window. In order to make the average value statistically significant, we should use an observation window of size $W > 10 \times$ max lag $= 300$.
But at these heart rates 300 beats correspond approximately to 2 minutes. It goes without saying that this time interval is way too big since we want to infer a local quantity.
This is why then more than the ACF it would be interesting to study the *partial anti-correlation function* $R^{(p)}(\tau)$, a sort *conditional* autocorrelation function that removes the cumulative linear contributions of past lags by taking into account the value assumed by the time series in the middle points while performing the average value in (2.1).

$$R^{(p)}(1) = C\left(\mathrm{RR}\left(i\right), \mathrm{RR}\left(i-1\right)\right) = C(1) \tag{3.18}$$

$$R^{(p)}(\tau) = C\left(\mathrm{RR}(i+1+\tau) - P_{i,\tau}\left(\mathrm{RR}(i+1+\tau)\right), \mathrm{RR}(i+1) - P_{i,\tau}\left(\mathrm{RR}\left(i+1\right)\right)\right) \tag{3.19}$$

for $\tau \geq 2$ and $P_{i,\tau}(x)$ being an operator projecting x onto the linear subspace of Hilbert space spanned by $x_{i+1}, \dots, x_{i+\tau}$. The goal of the latter is essentially to give the best linear predictor, in the sense of reducing the mean squared error, of $x_{i+1+\tau}$ given the previous τ points[18].
The pACF is a very powerful tool to determine the max-lag of a linear AR process, since the subtraction of the projections in the arguments of the correlator puts every lag greater than the max one to zero. Anyway, like always in statistics, sample estimates of the pACF will never be exactly zero, but one can consider its lags negligible (5% significance level) if they are between the band delimited by $\pm\frac{1.96}{\sqrt{L}}$ (if $L > 30$) where L is the length of the time series. Keeping in mind that during exercise the Heart Rate is changing a lot and that we would like to extrapolate a relation that binds its macroscopic variation to the fluctuations around the trend, alias the HRV, we will implement a local analysis of the pACF taking inspiration from dynamical DFA.

We considered the 7 marathon run time series (summary with details in the following Table 3.1) and 17 of the 200 time series of runner 7 analyzed in section 2.

We first defined a sliding window of dynamical size $W = 10$ lag. For the first 3 lags we won't consider any significance threshold because the dynamical observation windows are not long enough. Each time, while the window slides along the whole time series, we additionally detrended the data with a polynomial of order m. Afterwards, we compute the pACF using the Levinson-Durbin recursion scheme[19]. We use as parameter for the max lag of fitting the order of the lag we want to compute. For example, if we want to

#	Duration (beats)	Distance (km)	Age (y)	Weight (kg)	Height (cm)	Max HR (bpm)	Rest HR (bpm)	Sex
4	40034	41913.20	39	86	180	194	55	MALE
1	43771	42870.10	43	82	177	200	55	MALE
2	37027	42481.00	50	78	184	200	50	MALE
3	32200	42604.50	34	85	183	195	50	MALE
6	36880	41522.40	28	68	180	198	58	MALE
7	38270	42752.10	50	84	178	174	46	MALE
8	36262	41644.20	53	73	178	185	56	MALE

Table 3.1: Summary of the analyzed marathon time series.

calculate with dynamical pACF-m (with m being the detrending order, and $m = 1$) $R^{(p)}(3)$ we will set a $W = 30$ and take only the last value (lag = 3) of the pACF computed with the Levinson-Durbin algorithm with max fitted lag = 3.
Indeed, given a set of coefficients $\phi_{i,j}$, for a fixed lag k the $\phi_{i,j}$ satisfy the Yule-Walker equations[18]:

$$\rho_j = \phi_{k,1}\rho_{j-1} + \phi_{k,2}\rho_{j-2} + \phi_{k,3}\rho_{j-3} + \cdots + \phi_{k,k}\rho_{j-k} \tag{3.20}$$

where ρ_j are estimates of the ACF, and $i, j \leq k$.
The values $\phi_{k,k}$, varying k, are the partial autocorrelation function $R^{(p)}(k)$. At the same time the best linear predictor for the time series at time t given the previous k points, whether the process is autoregressive or not, will be:

$$\hat{x}_t = \phi_{k-1,1}x_{t-1} + \phi_{k-1,2}x_{t-2} + \cdots + \phi_{k-1,k-1}x_{t-1} \tag{3.21}$$

In this sense there is a direct link between the pACF and the coefficients of an AR process. Carrying forward the analysis, we ended up with time depended dynamical estimates of the pACF values $R^{(p)}(\tau, k)$, where the discrete index k spans the time series.
For each τ we have a time series describing the time evolution of that specific lag. We plot the results in a convenient color based fashion for the first 10 lags for the runner 7 time series and for the first 20 lags for the marathon ones (Figures 3.16, 3.17, 3.18, 3.19, 3.20, 3.21). Only values that are statistically non-zero according to their relative 5% significance threshold are plotted.

Remark 9 *We can make the followings remarks:*

1. *High intensity in a lag could be interpreted as the onset of a delayed regulatory mechanism or physiologic rhythm.*
2. $R^{(p)}(1)$ *and* $R^{(p)}(2)$ *are significantly negative across the whole time series.*
3. *In some parts also other* $R^{(p)}(i)$ *with* $i < 10$ *become negative. These can be seen as the couplings with the vascular and body temperature regulations. They are often followed by positive correlations in higher order lags.*

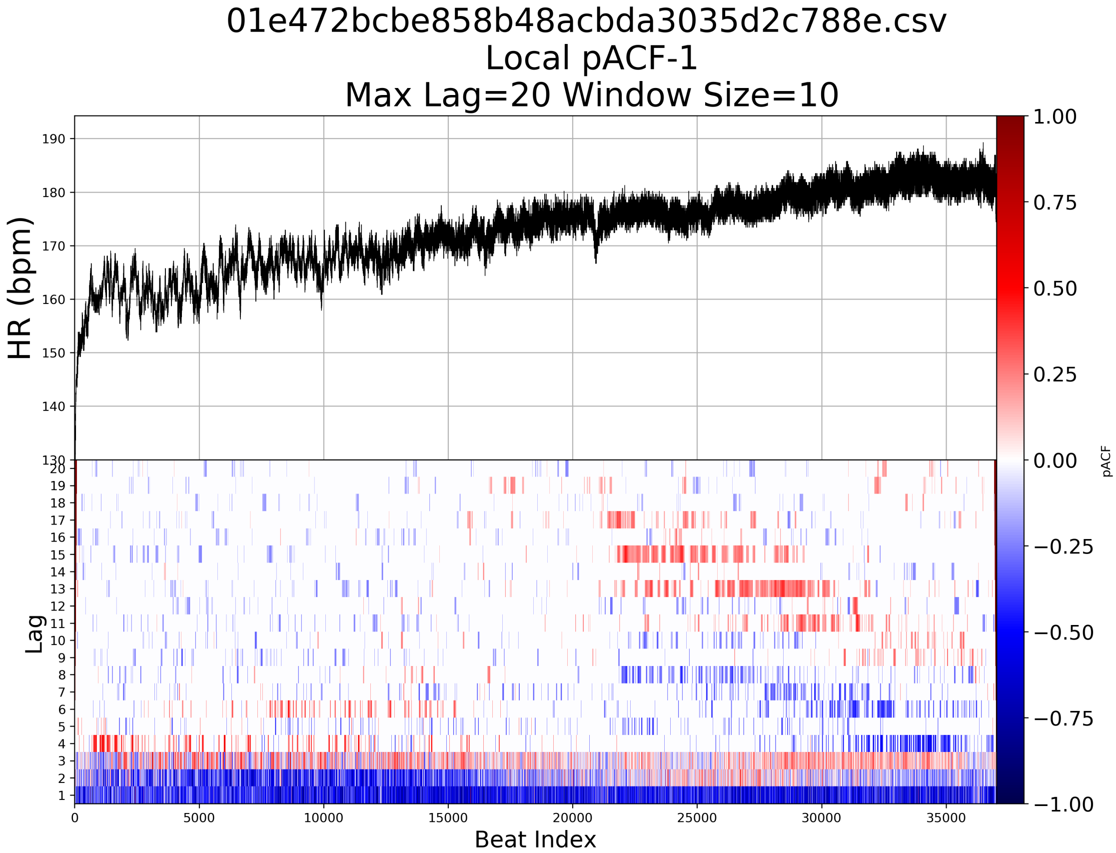

Figure 3.16: Dynamical pACF-1 up to lag 20 computed on marathon number 1. In the upper panel the time series is plotted, in the lower panel each line corresponds to the time evolution of a given lag within its dynamical window of size 10lag.

4. *If in some temporal intervals a set of lags is more prominent than others, and then this behavior changes, it can mean that those specific mechanisms were suppressed or that the frequencies of their oscillations had shifted.*

3.4 Conclusion

Every single one of the used approaches, within its range of validity, leads to the same conclusion: during exercise the fluctuations become anti-correlated.
The increase for HRV claimed in [2][3] appears to be probably due to the fact that the data have been fitted with an AR model. We have seen that this error comes from the arise of peaks in the *high frequency range* of the spectral density.
With the local-pACF method we also found out that the period of the dominant oscillation is changing in time.

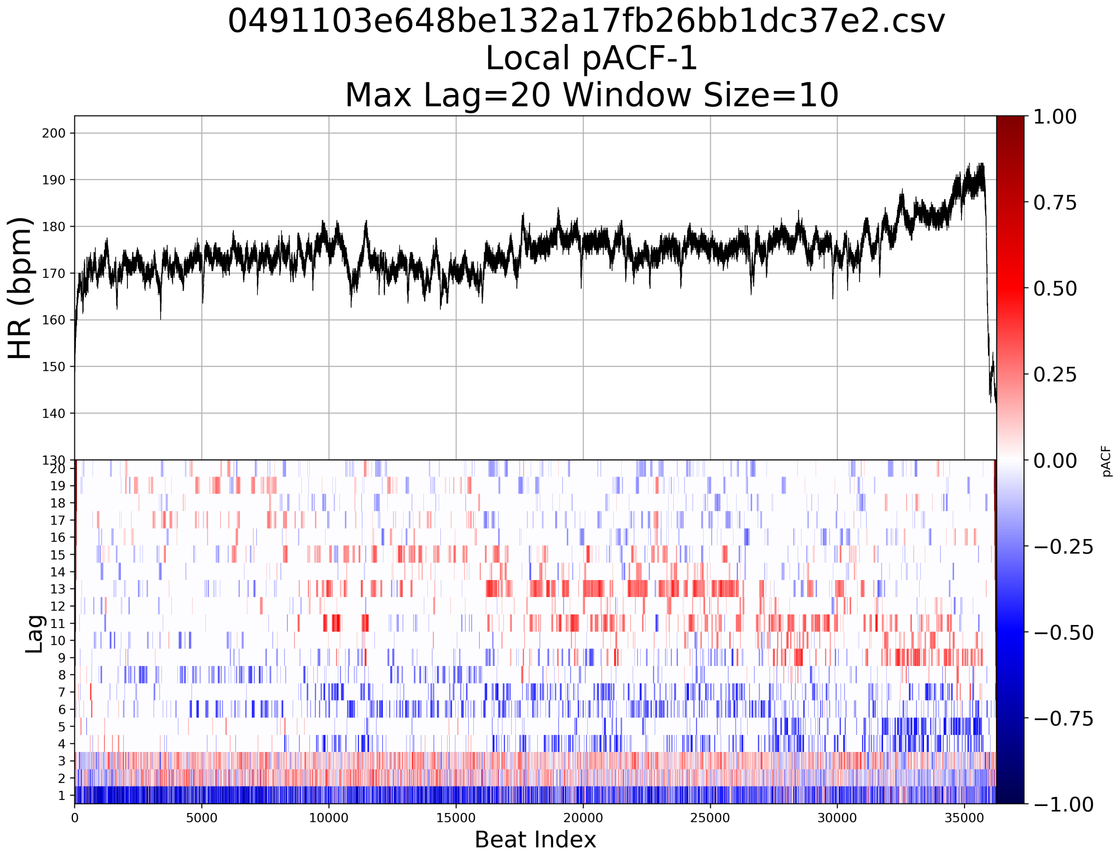

Figure 3.17: Dynamical pACF-1 up to lag 20 computed on marathon number 2. In the upper panel the time series is plotted, in the lower panel each line corresponds to the time evolution of a given lag within its dynamical window of size 10lag.

Local-DFA agrees with our findings: for short time scales the estimated local Hurst exponent H_t suggests that the data are generated by an anti-correlated stochastic process, and the fluctuations in H_t could be born from the shifts in frequency and amplitude of the spectral peaks related to the physiologic regulatory rhythms. Unfortunately we could not find a quantitative relation between HRV and the instantaneous heart rate. We should not forget that in order to achieve a precise result, we should also use a more rigorous detrending algorithm. An attempt towards this direction will be made in the following chapter.

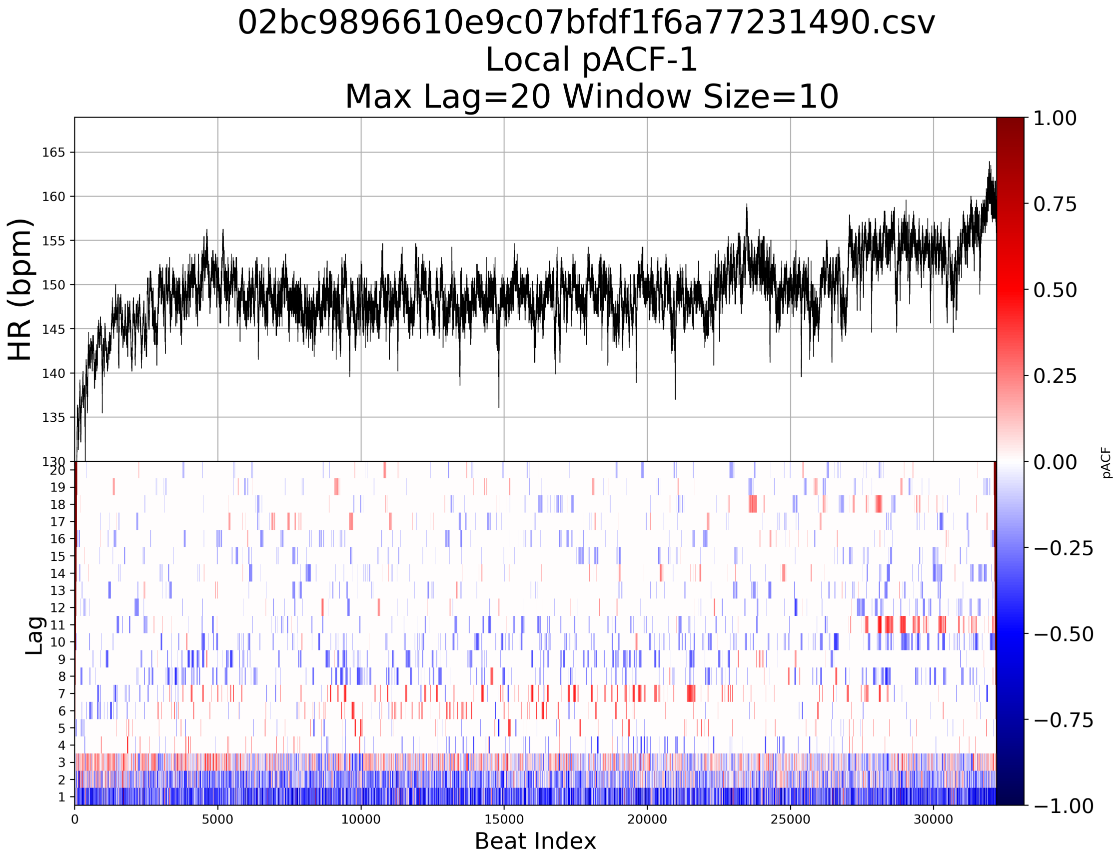

Figure 3.18: Dynamical pACF-1 up to lag 20 computed on marathon number 3. In the upper panel the time series is plotted, in the lower panel each line corresponds to the time evolution of a given lag within its dynamical window of size 10lag.

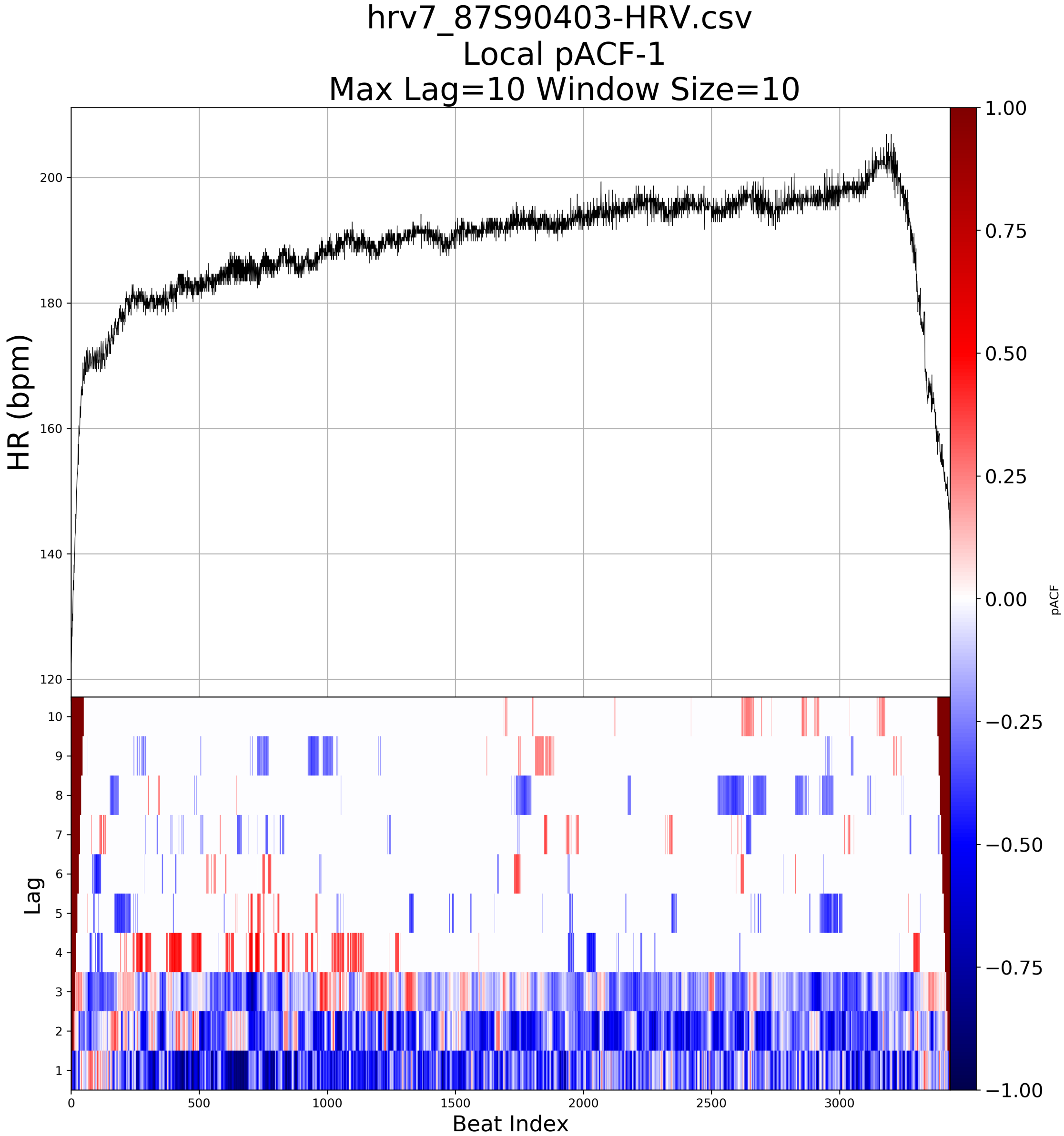

Figure 3.19: Dynamical pACF-1 up to lag 10 computed on a time series with a smooth exponential trend and final relaxation. In the upper panel the time series is plotted, in the lower panel each line corresponds to the time evolution of a given lag within its dynamical window of size 10lag.

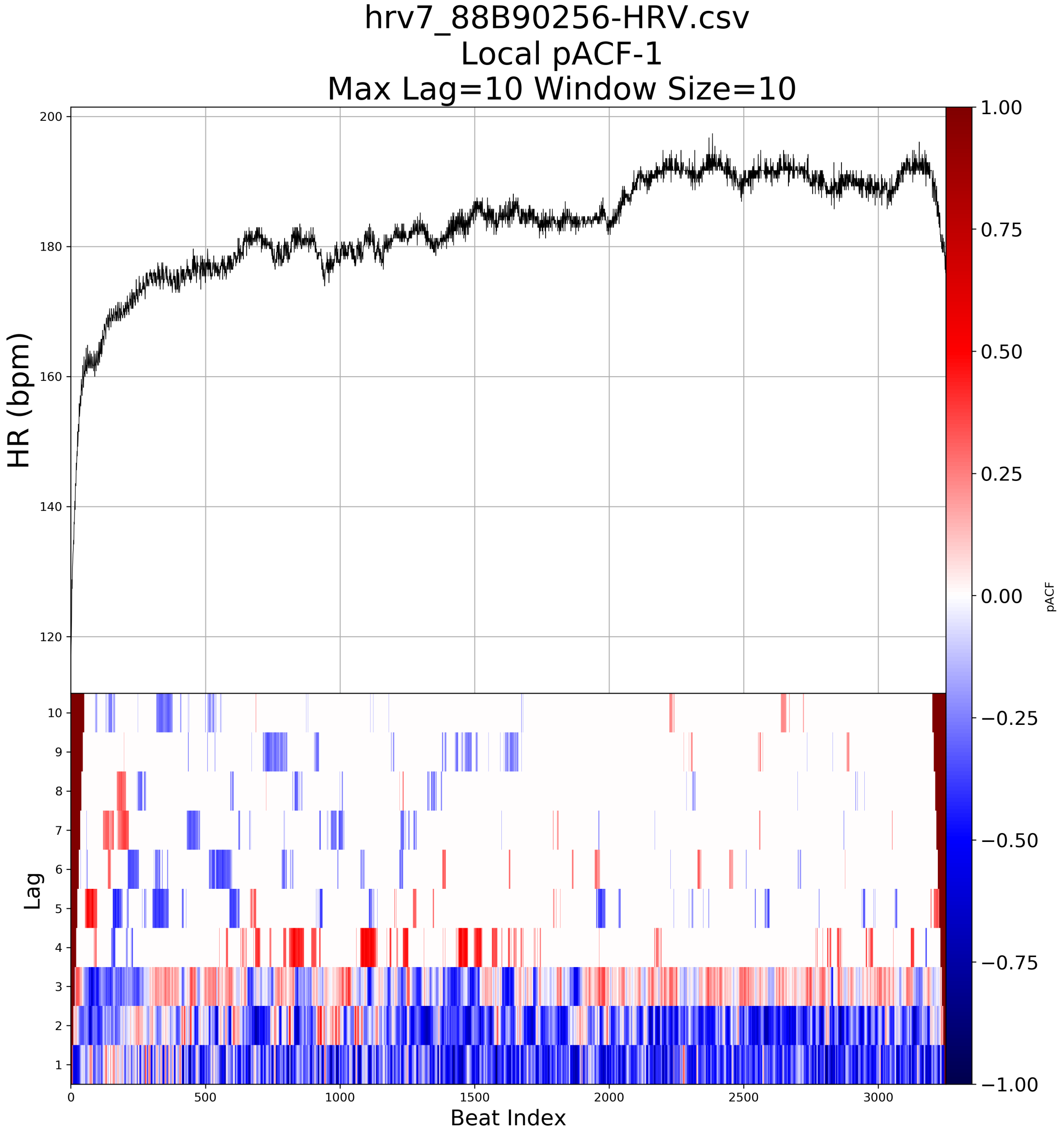

Figure 3.20: Dynamical pACF-1 up to lag 10 computed on a time series with an exponential trend plus some steep fluctuations. In the upper panel the time series is plotted, in the lower panel each line corresponds to the time evolution of a given lag within its dynamical window of size 10lag.

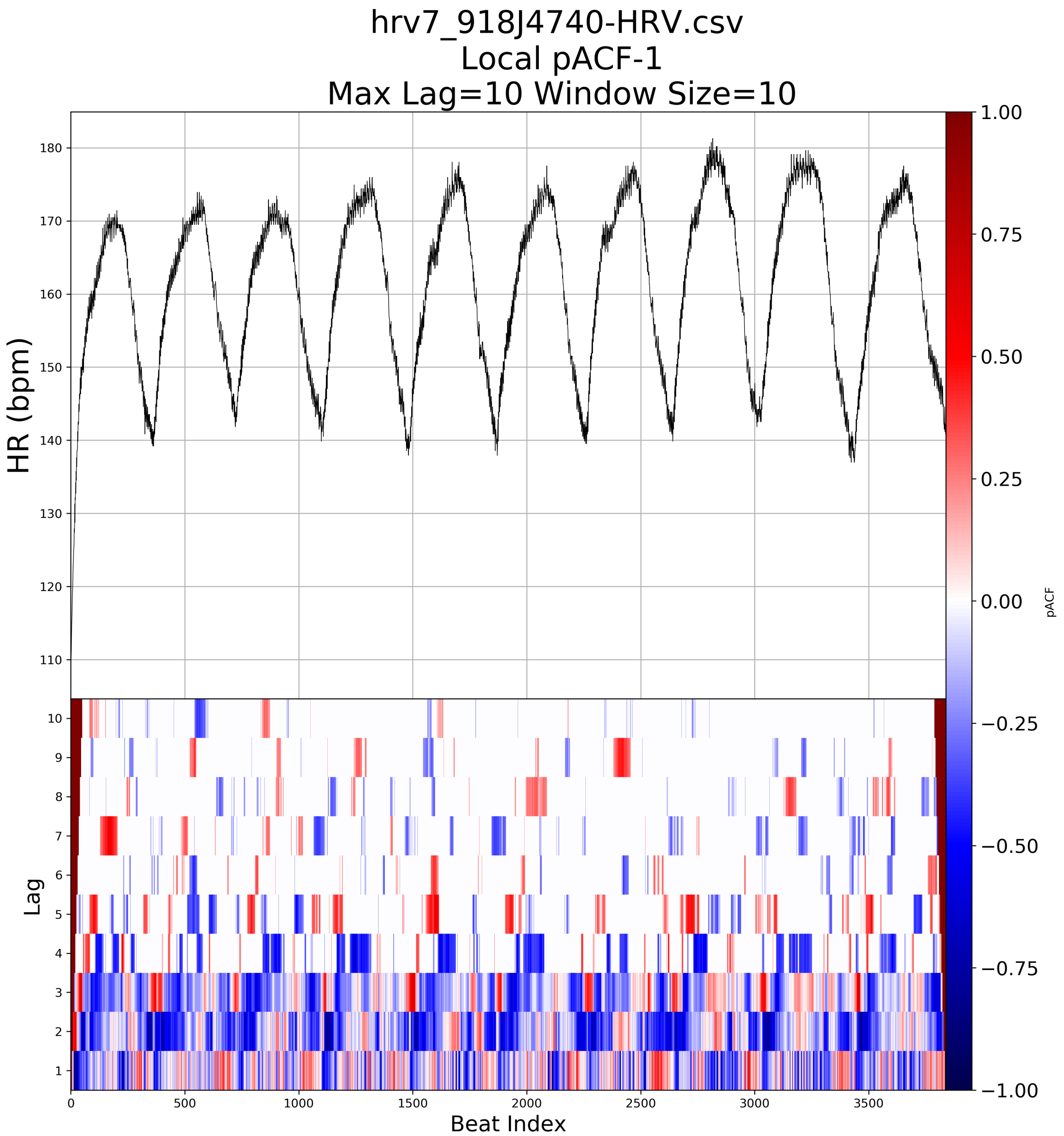

Figure 3.21: Dynamical pACF-1 up to lag 10 computed on a time series with a sequence of accelerations and decelerations. In the upper panel the time series is plotted, in the lower panel each line corresponds to the time evolution of a given lag within its dynamical window of size 10lag.

Chapter 4

Empirical Mode Decomposition

In this Chapter I will discuss Empirical Mode Decomposition[26], a completely algorithmic, data driven, approach for the frequency (mode) decomposition of short non-stationary time series.
This algorithm has been widely used in several different fields achieving outstanding results both in detrending and denoising. Usually the results are characterized by higher SNR ratios with respect to denoising and detrending performed with other techniques as Fourier Decomposition or Wavelet Analysis.
In the first section I will outline how the algorithms worked and how it has been improved during the years, reaching its current version called Complete Ensemble Empirical Mode Decomposition with Adaptive Noise *CEEMDAN*[27][28].
In the second section I will outline the Hilbert-Huang Transform and the subsequent Hilbert-Huang Spectral Analysis.
Finally, in the last section the applications to RR time series recorded during exercise will be discussed.

4.1 The algorithm

The goal of the EMD algorithm is to decompose the signal in a list of Intrinsic Mode Functions or *IMF* plus a Residual trend. The IMF will be full-fledged wide-sense periodic stationary time series characterized by an almost constant in time frequency and a varying amplitude. The residual trend often contains the part of the time series that is not mean reverting.
To extract the IMF the following sifting process must be applied:

1. Identify all the local maxima and minima in the data

2. Interpolate with a cubic spline the upper and lower envelopes as the curves passing through all the maxima and that passing through all the minima

3. Compute the average envelope m_1 as the average curve between the previous two interpolated curves

4. Subtract the average envelope from the data (Figure 4.1):

$$X(t) - m_1 = h_1 \tag{4.1}$$

5. Reiterate, this time using h_1 as an input, until at the k iteration the number of consecutive siftings for which the number of zero-crossings and extrema are equal or at most differing by one is less than a previously chosen parameter called S-number (that is usually an integer between 4 and 8). Huang found out that in this way the algorithm works best. [29]

$$\begin{aligned} h_1 - m_{11} &= h_{11} \\ &\dots \\ h_{1(k-1)} - m_{1k} &= h_{1k} \end{aligned}$$

6. Set $\mathrm{IMF}_1 = h_{1k}$

7. Reiterate the siftings process with $r_1 = X(t) - \mathrm{IMF}_1$ as an input and find all the remaining IMF and the residual.

8. We finally obtain:

$$X(t) = \sum_{i=1}^{n} \mathrm{IMF}_i + r_n \tag{4.2}$$

What is the significance of the IMF? The algorithm doesn't look like it has a solid mathematical background and the IMF are not orthogonal in the sense of the dot product of the l^2 vector space. Yet they somehow encode better the real nonlinear submodes that compose a signal if there are no spikes. Recently Niang has tried to analytically formalize how the procedure works using partial differential equations [25]
Anyway the phenomenon of mode-mixing, that is when a real signal divided into different spurious IMF, is yet present.
Many attempts have been done [27][28] in order to improve the decomposition quality. The most successful ones use zero average white noise to introduce a comparison scale that the algorithm will exploit to discern better between modes since this kind of noise is made of a wide spectrum of frequencies. The one performing best is called Improved CEEMDAN and works as follow:

- Before step 1 create N copies of the signal and add to them different realizations of white noise extracted from a normal distribution of zero mean, choosing the variance with the aim of having a particular ratio between the standard deviation of the noise and the standard deviation of the signal. After that compute the first IMF on all copies.

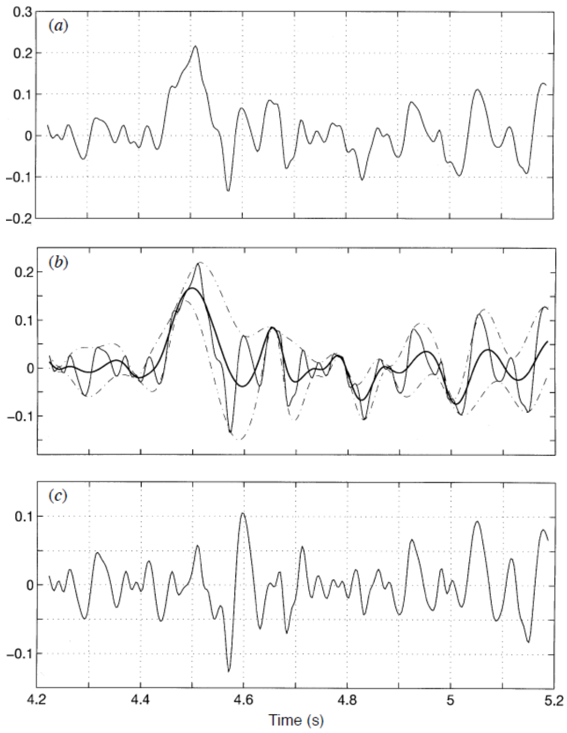

Figure 4.1: Example of firsts steps of sifting process. Taken from [26]

- Take an average of the computed IMF in order to cancel out the contributions given by the noise, this will be final IMF_1.
- Subtract IMF_1 from the signal, and reiterate on the residual, but adapting the variance time to time as to having the original ratio of the standard deviations fixed.

4.1.1 Example: highly non linear function

Let's now perform EMD and Improved CEEMDAN on the following functions defined in $t \in [0,1]$:

$$Y(t) = \cos\left(22\pi t^2\right) + 7t^2 \tag{4.3}$$

and

$$X(t) = \begin{cases} \cos\left(22\pi t^2\right) + 7t^2, & 0 \leq t < 0.9 \vee 0.9 < t \leq 1 \\ 0, & t = 0.9 \end{cases} \tag{4.4}$$

$X(t)$ is equal to $Y(t)$ except for a discontinuity at $t = 0.9$. In the numerical implementation t is a sequence of numbers between 0 and 1 and spacing $\delta = 0.001$.
On one hand EMD of $Y(t)$ gives almost an exceptionally good output with the cos and the parabolic trend perfectly separated (Figure 4.3), on the other EMD of $X(t)$ is mixing the discontinuity with the cos, it's creating spurious modes and it's also bad at detecting

the trend, which in this case looks to have the opposite concavity (Figure 4.4).
Eventually, CEEMDAN (with ensemble size = 1000 and noise strength = 0.2) of $X(t)$ is acceptably good. The first IMF carry most of the *energy* of the discontinuity. Unfortunately the cos is decomposed in more modes but the trend is well identified. Using CEEMDAN we might then consider that the original modes present in the signal might not be perfectly isolated if discontinuities are present (Figure 4.5).

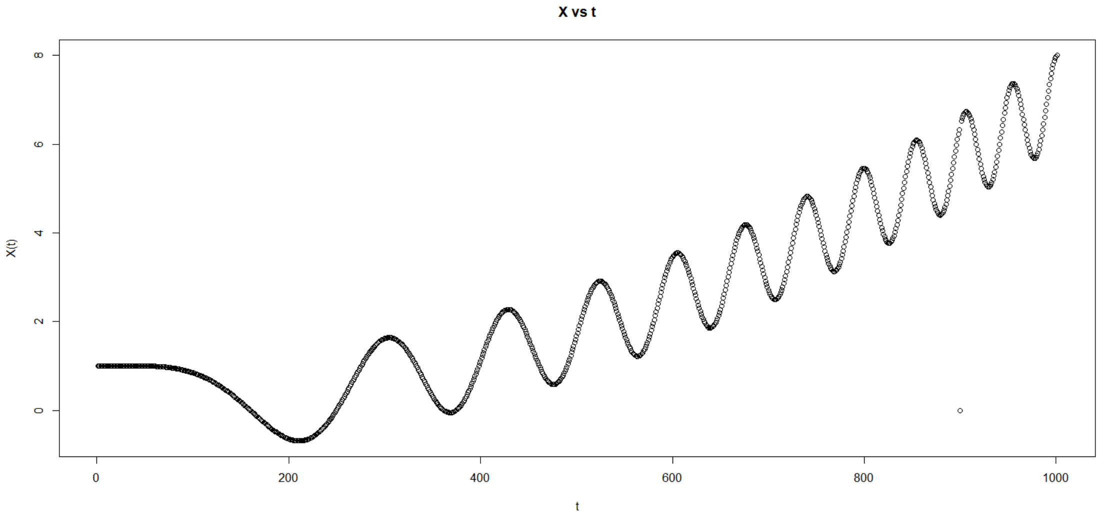

Figure 4.2: Function (4.4). Time axis counts the index in the discretized list.

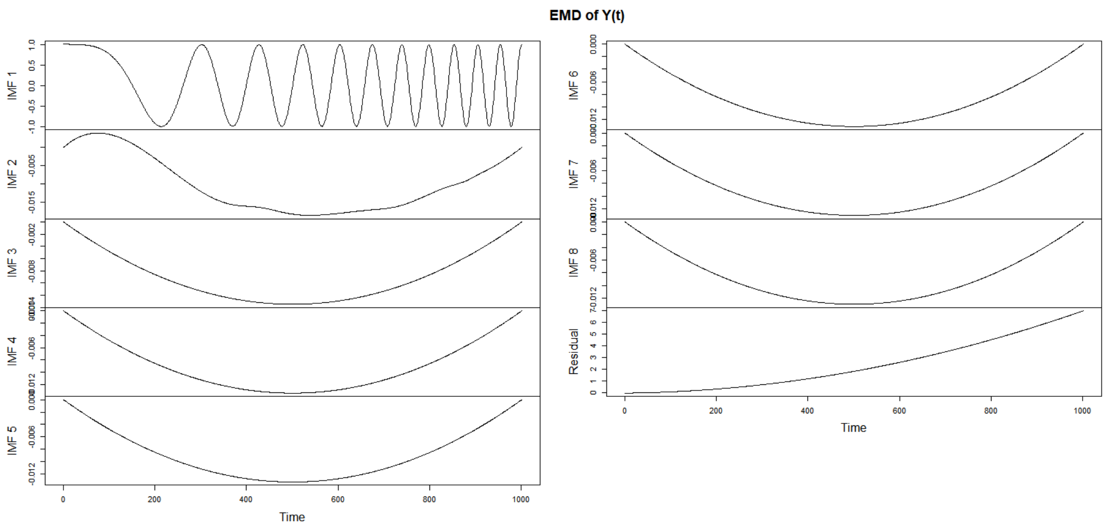

Figure 4.3: EMD on (4.3). Time axis counts the index in the discretized list.

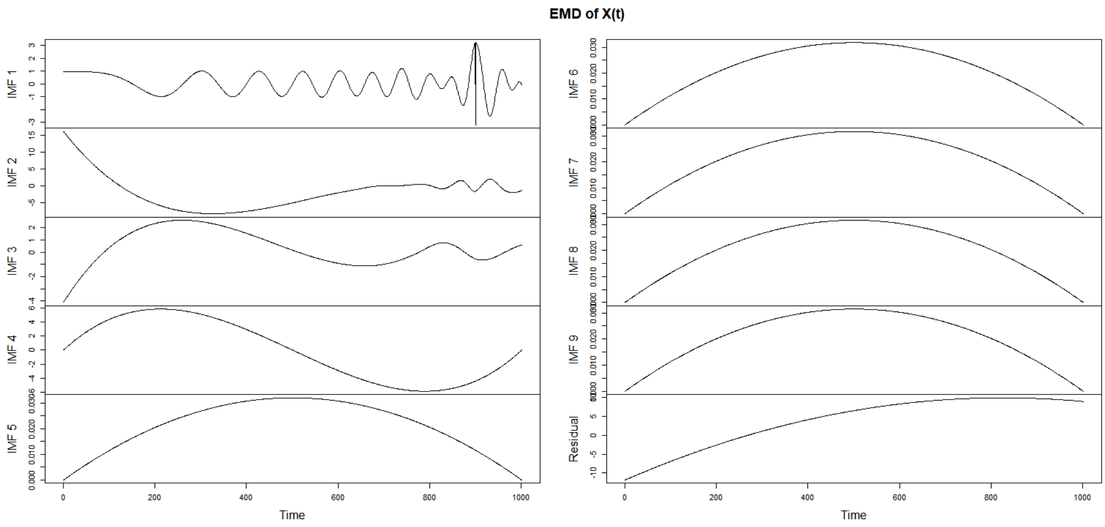

Figure 4.4: EMD on (4.3). Time axis counts the index in the discretized list.

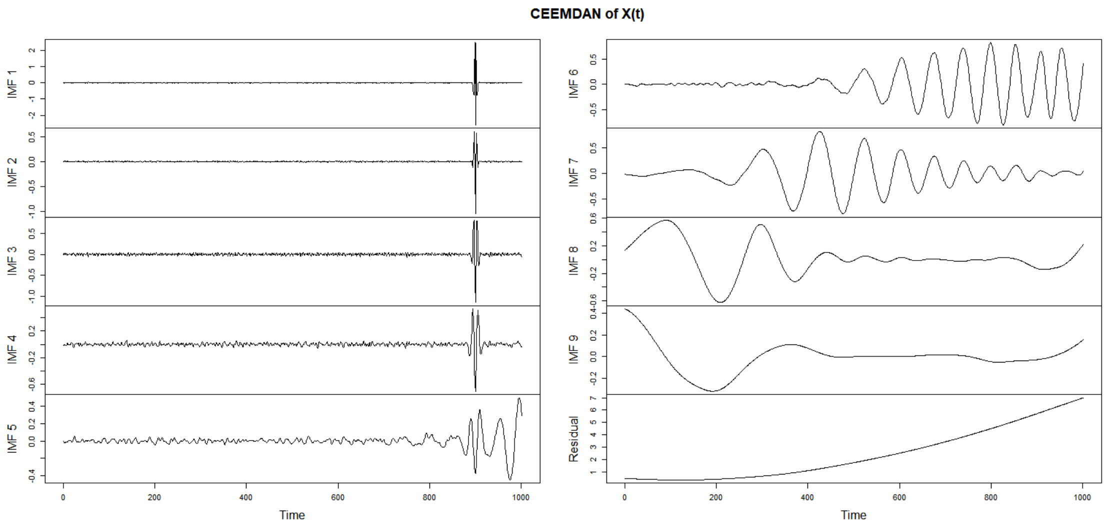

Figure 4.5: CEEMDAN on (4.4). Time axis counts the index in the discretized list.

4.2 The Hilbert Transform and Spectrum

The IMF contain all the information about the amplitude and the frequency of the selected oscillating modes and how they change with time. Extracting this information can be done with the Hilbert transform.

Being $Y(t)$ the Hilbert Transform of a function $X(t)$:

$$Y(t) = \frac{1}{\pi} P \int_{-\infty}^{\infty} \frac{X(t')}{t - t'} dt' \tag{4.5}$$

one can define the complex signal as:

$$S(t) = X(t) + iY(t) = a(t)e^{i\theta(t)} \tag{4.6}$$

and eventually one can define an instantaneous frequency $\omega(t)$ as

$$\omega(t) = \frac{d\theta(t)}{dt} \tag{4.7}$$

The generalization to discrete signals is straightforward. One then can study the time evolution of the *instantaneous* amplitude $a(t)$ and frequency $\omega(t)$ of each IMF.
The time evolution of the sum of the amplitude/frequency relation over all IMF is called the Hilbert spectrum and indeed performing the Hilbert Transform over all IMF the original time series can be written in the following form:

$$S(t) = \sum_{j=1}^{k} a_j(t)\, e^{i \int \omega_j(t') dt'} \tag{4.8}$$

Simple Fourier Decomposition would have led to a similar expression but with constant a_j and ω_j. Amplitude and frequency adaptability makes the Hilbert-Huang transform more suitable for the analysis of non-linear, non-stationary time series.
We define the Hilbert Spectrum of each IMF in this way:

$$H_j(\omega, t) = \begin{cases} a_j(t), & \omega_j(t) = \omega \\ 0, & \text{else} \end{cases}$$

And the Hilbert spectrum of the total signal $X(t)$ is:

$$H(\omega, t) = \sum_{j=1}^{k} H_j(\omega, t) \tag{4.9}$$

4.3 Application to RR time series

I will now show some results of the application of the Hilbert-Huang Spectral Analysis to the marathon time series analyzed in the previous chapter. The decomposition has been performed using the CEEMDAN function from Rlibeemd package[30] with ensemble size = 1000 and noise strength = 0.2.

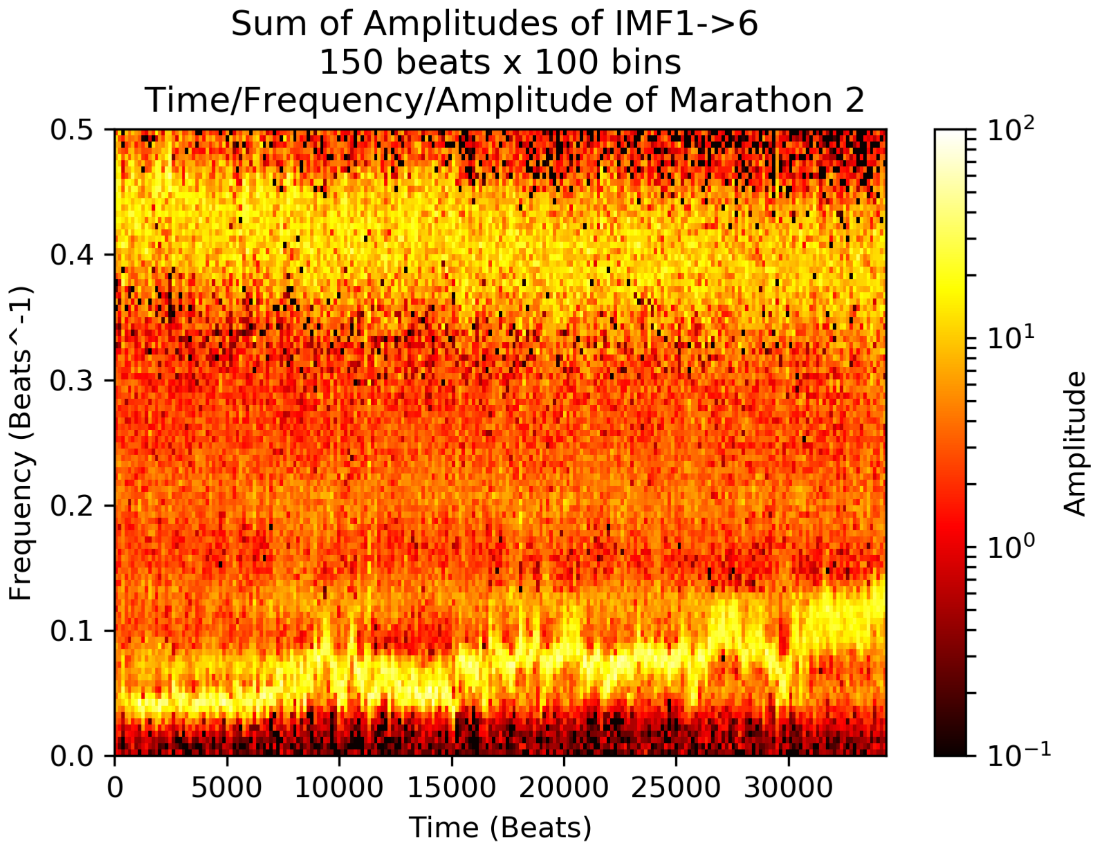

Figure 4.6: Hilbert Spectrum of the sum of the first 6 IMF of marathon file number 2. For graphical purposes the frequency axis has been divided into 150 bins and the time axis into bins of size $L = 100$.

Remark 10 *From the Figures (4.6, 4.7, 4.8) we can clearly see a high intensity frequency very broad band around* $\omega = 0.5$ *beats*$^{-1}$ *and some more narrow ones at lower* ω*. It's clear that the amplitude and average frequency is shifting in time. This is because the underlying process is highly non-linear and non-stationary and it's also the main reason why simple Fourier Spectral Analysis does not perform well.*

It's also interesting to plot the Hilbert Spectrum where the time axis is replaced by the instantaneous HR assumed by the time series at each instant. (Figures 4.9, 4.10, 4.11).

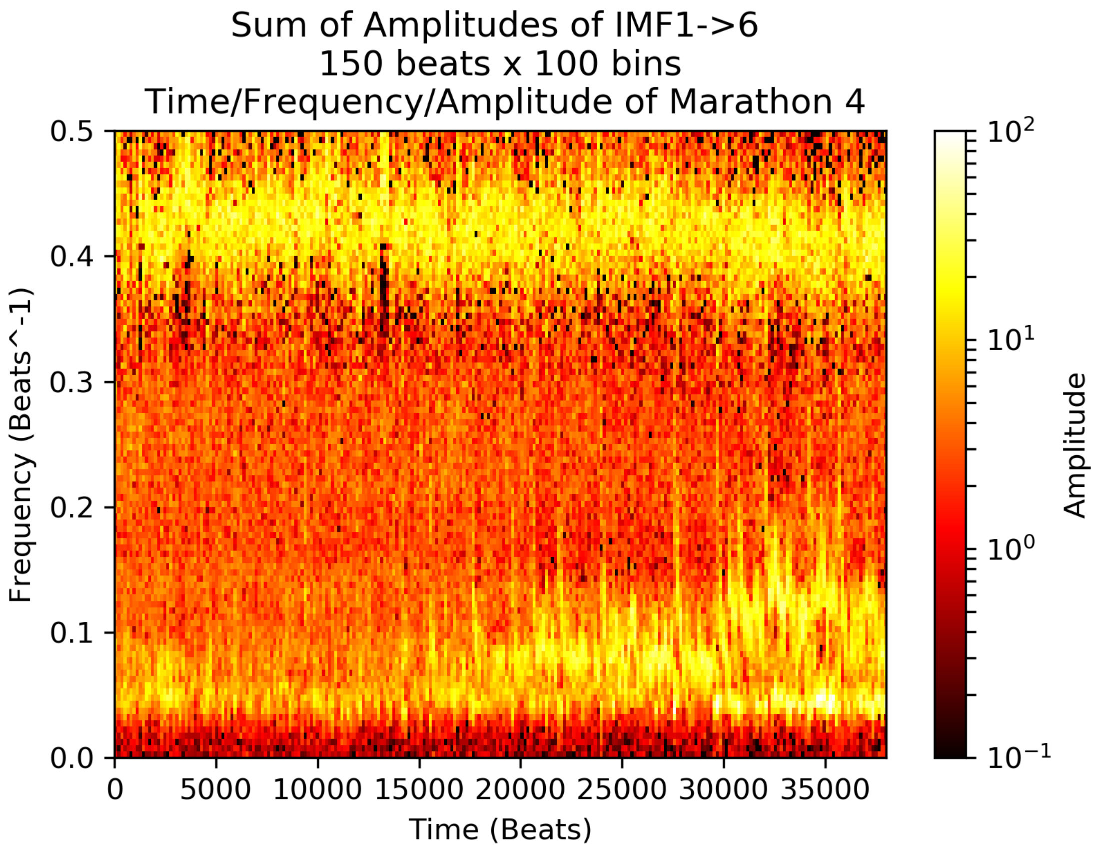

Figure 4.7: Hilbert Spectrum of the sum of the first 6 IMF of marathon file number 4. For graphical necessities the frequency axis has been divided into 150 bins and the time axis into bins of size $L = 100$.

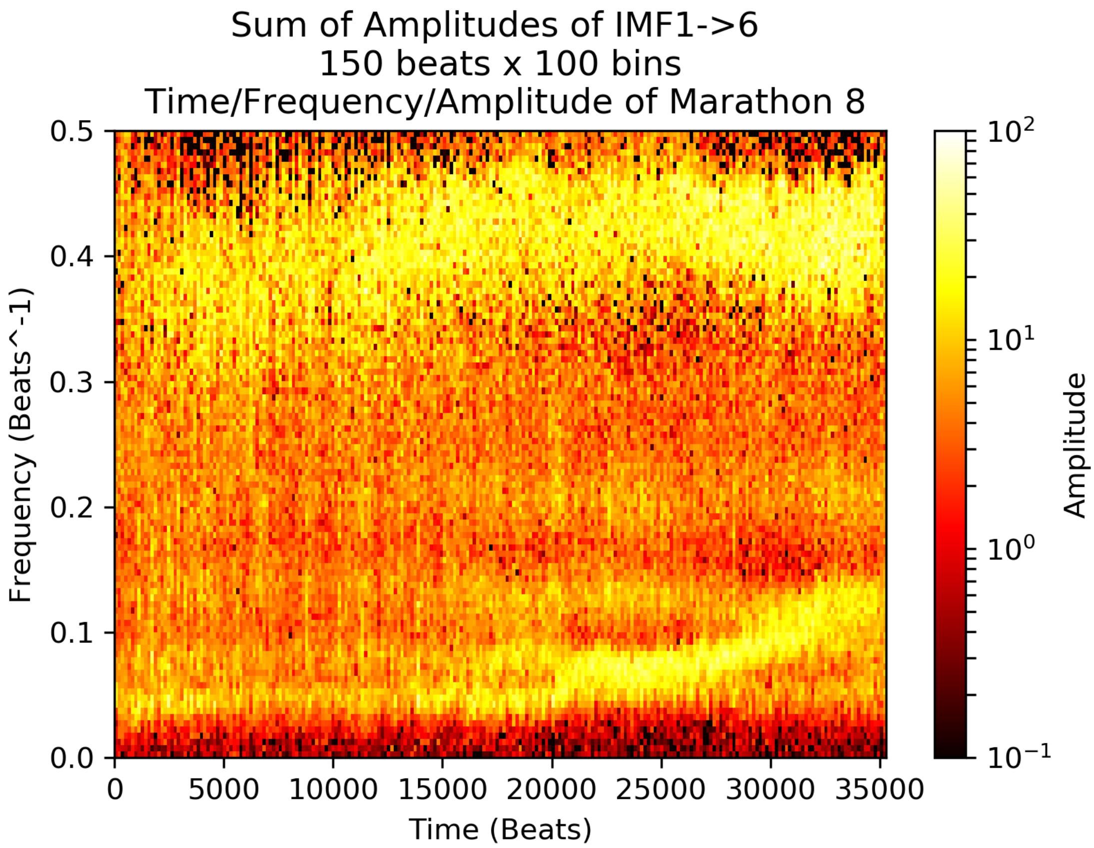

Figure 4.8: Hilbert Spectrum of the sum of the first 6 IMF of marathon file number 8. For graphical necessities the frequency axis has been divided into 150 bins and the time axis into bins of size $L = 100$.

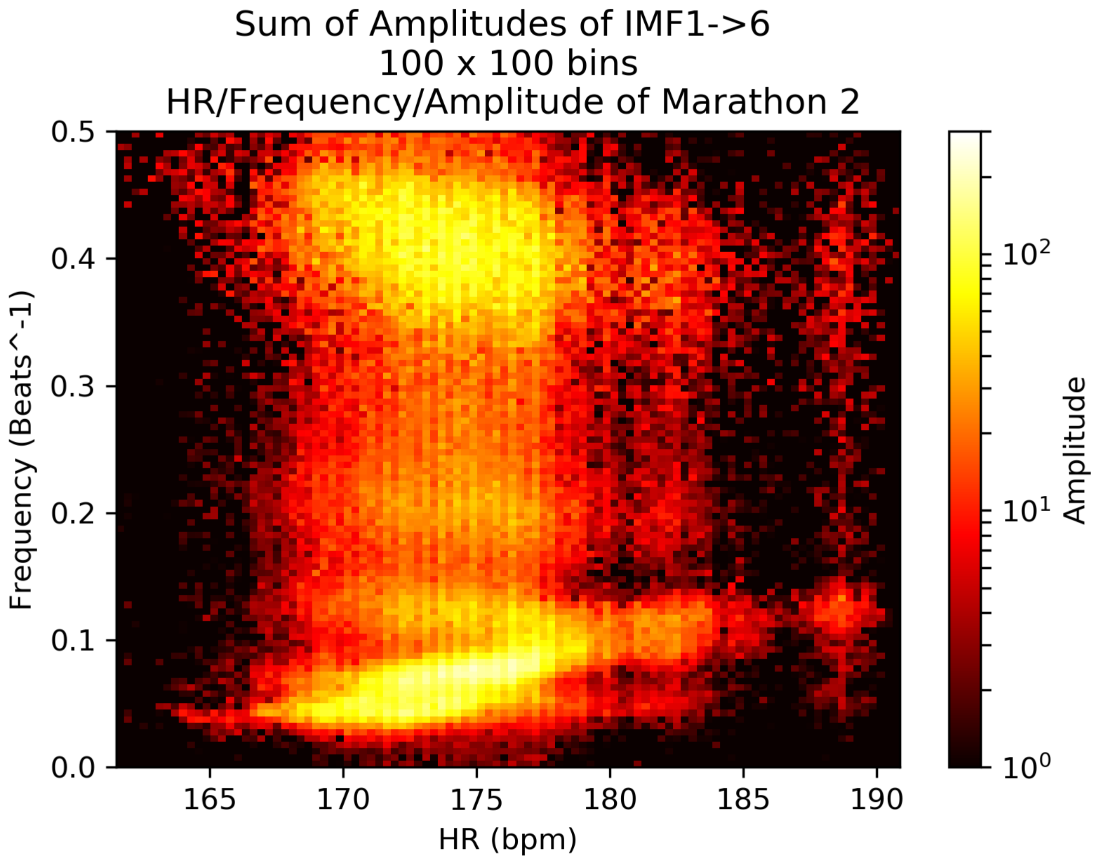

Figure 4.9: Hilbert Spectrum with respect to the instantaneous HR of the sum of the first 6 IMF of marathon file number 2. For graphical necessities the axis has been divided into 100 bins.

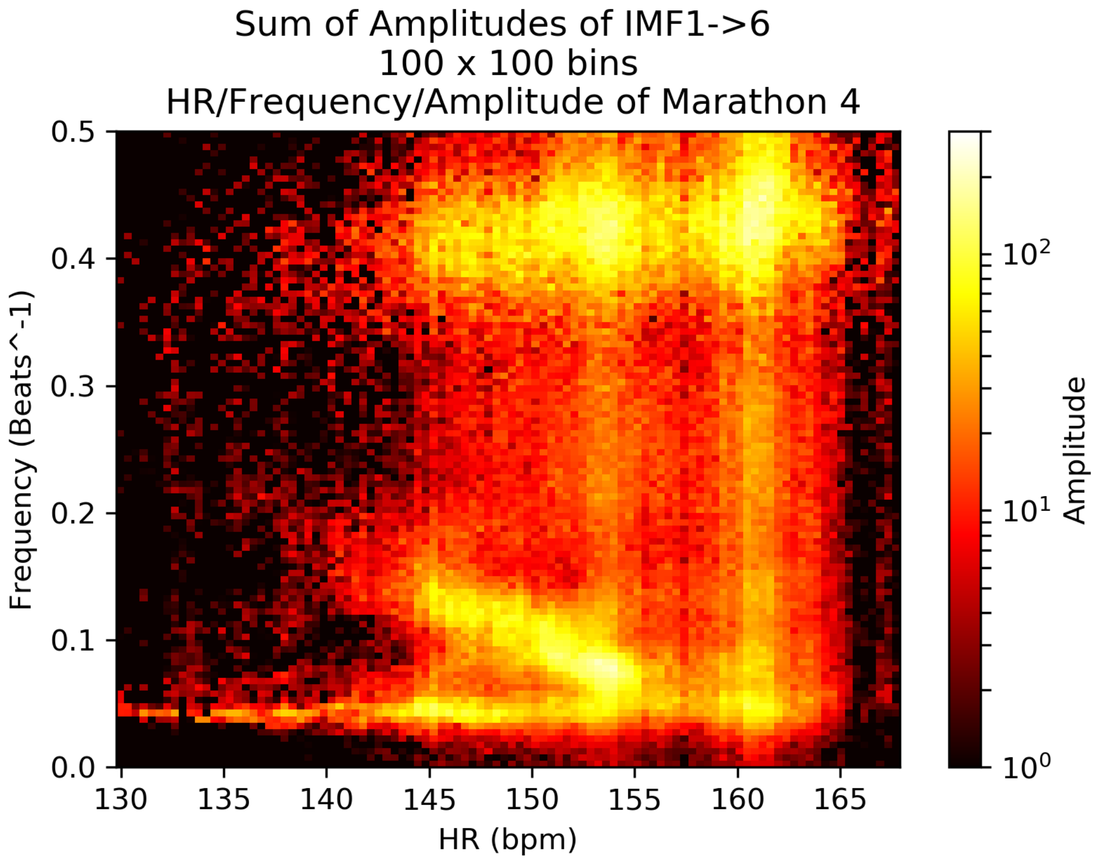

Figure 4.10: Hilbert Spectrum with respect to the instantaneous HR of the sum of the first 6 IMF of marathon file number 4. For graphical necessities the axis has been divided into 100 bins.

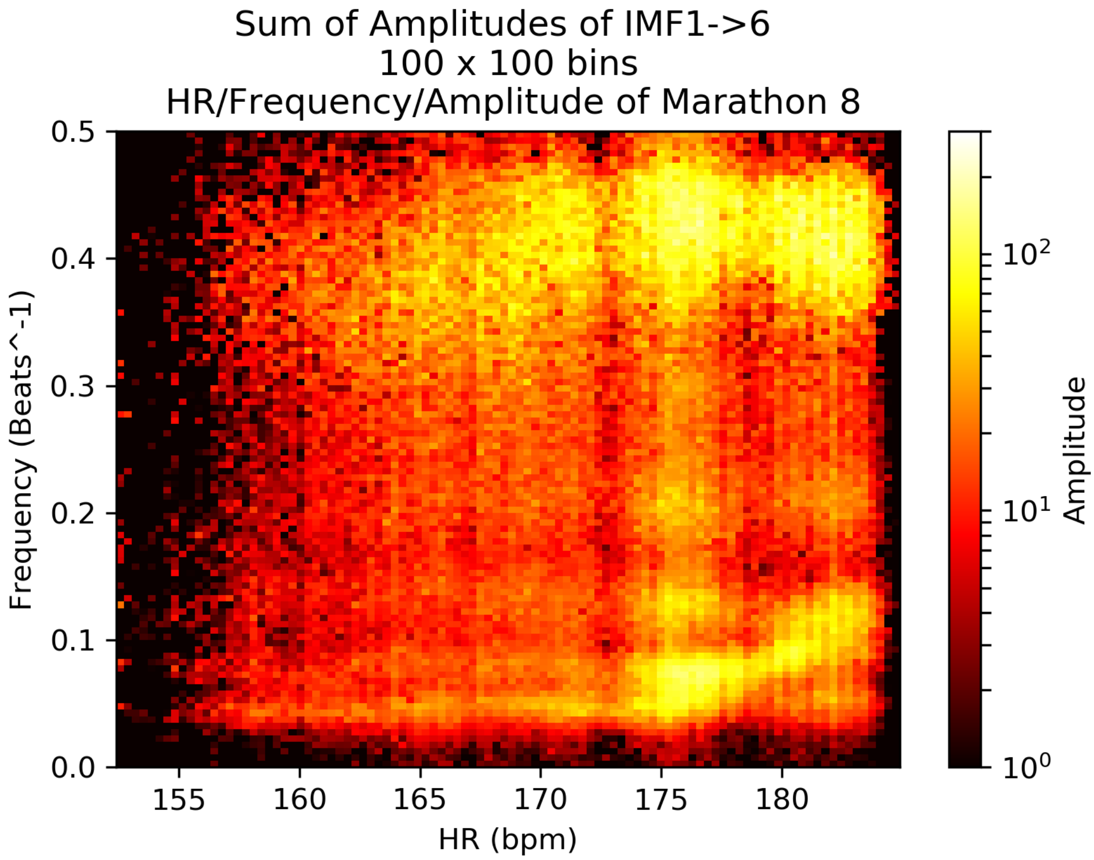

Figure 4.11: Hilbert Spectrum with respect to the instantaneous HR of the sum of the first 6 IMF of marathon file number 8. For graphical necessities the axis has been divided into 100 bins.

Chapter 5

Conclusion and perspectives

Heart rate variability is a very important quantity that can give us a view on the health status of a patient. In this master thesis, I have focused my attention on the study of the Heart Rate Variability in time series recorded during physical exercise, exploiting the relation between the fluctuations and the correlations along the data. Since the current state of art in the field does not provide a unique efficient tool that can be used to perform the analysis, I made use of many of them: Auto Regressive fitting, Dynamical Detrended Fluctuation Analysis, Dynamical Partial Autocorrelation Function (that I developed during the work) and Hilbert-Huang Spectral Analysis. When using these techniques, an extreme attention was given to their range of validities and their limitations, stressing out how and where the methods could be used. The results of each approach have been interpreted with extreme care and consistently pointed out that the analyzed data benefits of a deep, intrinsic complexity. The RR time series recorded during physical activity are characterized by strongly anti-correlated fluctuations that I believe are caused by the dynamical coupling with physiologic regulatory cycles that serve to balance the beating rate when the heart is under stress, also adjusting it according to the respiratory cycle and to vascular pressure and temperature changes. Both the coupling intensity and the cycle frequency appear to be shifting in time in a non trivial fashion. Unfortunately, at the moment I could not extract a quantitative precise relation that links the amplitude or the frequencies of the fluctuation to the instantaneous Heart Rate, still this internship work was very productive because I was able not only to show the presence of these high frequency modes in the signal, but also to shed light on the DFA and its link to an autoregressive process and to the partial autocorrelation function. All the used approaches, anyway, are very sensitive to the detrending process effectuated in order to remove the stochastic fluctuations that are not strictly generated by the heart and by its numerous parasympathetic regulatory mechanisms. I am confident that in the near future further studies might be able to find some analytical relation between the coupling intensity and the heart rate, especially if Empirical Mode Decomposition will be further improved.

Bibliography

[1] C. Chatfield (1989),*The Analysis of Time Series—An Introduction (fourth ed.)*, Chapman and Hall, London. pp. 94–95. ISBN 0-412-31820-2.

[2] K. Takata, Y. Watanabe, H. Kakeno (1983), *Time Series Analysis of R-R Interval Variability during Running Load in Man [Article in Japanese]*, Iyodenshi To Seitai Kogaku. 1984 Jun;22(3):194-8.

[3] K. Takata, Y. Watanabe, K. Yokoyama (1988), *Quantification of the Heartbeat Rhythm Using Characteristic Equation of Autoregressive Model of R-R Intervals in ECG*, Systems and Computers in Japan, Vol. 20, No. 4, 1989

[4] R. Avram *et al.* (2018), *Redefining Normal Resting Heart Rate Values Using Big Data*, AHA Journals, Circulation. 2018;138:A15098

[5] A.L. Goldberger, H.E. Stanley *et al.* (2002), *Fractal dynamics in physiology: Alterations with disease and aging*, PNAS February 19, 2002 99 (suppl 1) 2466-2472

[6] G. Captur, A.L. Karperien, A.D. Hughes, D.P. Francis, J.C. Moon (2016), *The fractal heart - embracing mathematics in the cardiology clinic*, Nature Reviews Cardiology, October 2016

[7] H.E. Hurst (1951), *Long-term storage capacity of reservoirs*, Transactions of American Society of Civil Engineers. 116: 770.

[8] K. Kiyono (2015), *Establishing a direct connection between detrended fluctuation analysis and Fourier analysis*, arXiv:1508.02204v4 [physics.data-an]

[9] C.K. Peng *et al.* (1994), *Mosaic organization of DNA nucleotides*, Phys. Rev. E. 49: 1685-1689

[10] C.K. Peng, S. Havlin, H.E. Stanley, A.L. Goldberger (1994), *Quantification of scaling exponents and crossover phenomena in nonstationary heartbeat time series*, Chaos An Interdisciplinary Journal of Nonlinear Science. Volume 5, Issue 1. 10.1063/1.166141)

[11] H.E. Stanley *et al.* (2001), *Effect of Trends on Detrended Fluctuation Analysis*, arXiv:physics/0103018v4

[12] H.E. Stanley *et al.* (2002), *Effect of nonstationarities on detrended fluctuation analysis*, Phys. Rev. E. 65: 041107

[13] L. Xu, P.C. Ivanov, K. Hu, Z. Chen, A. Carbone, H.E. Stanley (2005), *Quantifying signals with power-law correlations: A comparative study of detrended fluctuation analysis and detrended moving average techniques*, Physical Review E 71, 051101

[14] E.A.F. Ilhen (2012), *Introduction to multifractal detrended fluctuation analysis in Matlab*, Frontiers in Physiology, June 2012 , Volume 3, Article 141

[15] M. Javorka, I. Žila, T. Balhárek, K. Javorka (2002), *On- and off-responses of heart rate to exercise – relations to heart rate variability*, Clinical Physiology and Functional Imaging 23, 1, 1–8

[16] J.W. Kantelhardt (2008), *Fractal and Multifractal Time Series*, arXiv:0804.0747v1

[17] B. Tóth, J. Kertész (2005),*Increasing market efficiency: Evolution of cross-correlations of stock returns*, arXiv:physics/0506071v2, physics.soc-ph

[18] G.E. P. Box, G.M. Jenkins, G.C. Reinsel (2008), *Time Series Analysis, Forecasting and Control (4th ed.)*, Hoboken, NJ: Wiley.

[19] J. Durbin, (1960), *The fitting of time series models*, Rev. Inst. Int. Stat. , v. 28, pp. 233–243.

[20] P.G. Meyer, H. Kantz (2019), *Inferring characteristic timescales from the effect of autoregressive dynamics on detrended fluctuation analysis*, New J. Phys. 21 033022

[21] W.E. Dean Jr. , R.Y. Anderson (1974), *Application of some correlation coefficient techniques to time-series analysis*, Journal of the International Association for Mathematical Geology, December 1974, Volume 6, Issue 4, pp 363–372

[22] J.D. Scargle (1989), *Studies in astronomical time series analysis. III - Fourier transforms, autocorrelation functions, and cross-correlation functions of unevenly spaced data*, Astrophysical Journal, Part 1, vol. 343, Aug. 15, 1989, p. 874-887.

[23] J.W. Kantelhardt, Y. Ashkenazy, P. C. Ivanov, A. Bunde, S. Havlin, T. Penzel, J. Peter, and H.E. Stanley (2002), *Characterization of sleep stages by correlations in the magnitude and sign of heartbeat increments*, Phys. Rev. E 65, 051908

[24] H. Mand, H. Kantz (2015), *The relationship between the detrendend fluctuation analysis and the autocorrelation function of a signal*, Eur. Phy. J. B 88 327

[25] O. Niang *et al.* (2012), *Partial differential equation-based approach for empirical mode decomposition: application on image analysis.*, IEEE Transactions on Image Processing Volume: 21 , Issue: 9 , Sept. 2012

[26] N.E. Huang *et al.* (1998), *The empirical mode decomposition and the Hilbert spectrum for nonlinear and non-stationary time series analysis*, 454 Proc. R. Soc. Lond. A

[27] M.E. Torres, M.A. Colominas, G. Schlotthauer, P. Flandrin (2011), *A complete ensemble empirical mode decomposition with adaptive noise*, Acoustics, Speech and Signal Processing (ICASSP), pp. 4144–4147

[28] M.A. Colominas, G. Schlotthauer, M.E. Torres (2014), *Improved complete ensemble EMD: A suitable tool for biomedical signal processing*, Elsevier, Biomedical Signal Processing and Control 14 (2014) 19–29

[29] N.E. Huang *et al.* (2003), *A confidence limit for the empirical mode decomposition and Hilbert spectral analysis*, P Roy Soc Lond A Mat 4592317–2345

[30] P.J.J. Luukko, J. Helske, E. Räsänen (2017), *Introducing libeemd: A program package for performing the ensemble empirical mode decomposition*, arXiv:1707.00487v1 [stat.CO]